Article

Urbanization's dual role in the exacerbation and mitigation of drought dynamics in China

Check for updates
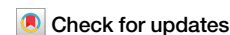
Karam Alsafadi[1]✉, Jiwei Sun[2], Irfan Ullah[3], Amit Kumar Srivastava[4], Frank Ewert[4,5], Boufeniza Redouane Larbi[6], Shuoben Bi[2], Shengchang Yang[1], Feifei Wang[1] & Wenzhi Cao[1]✉

Since the 1980s, China's rapid urbanization has profoundly influenced local drought conditions by altering ecological, environmental, and meteorological systems. However, the role of urbanization timing in shaping drought dynamics—particularly drought duration, severity, intensity, and frequency—remains underexplored. This study investigates the impacts of urbanization on drought characteristics across mainland China using a comprehensive dataset of weather station observations spanning 1951–2020. Stations were categorized based on their urbanization timing: early-urbanized (U_b: before 1985) and recently urbanized (U_a: after 1985). Results reveal that early-urbanized stations consistently exhibit drought exacerbation, especially for short-term drought frequency (ΔTND) and severity (ΔMDS, ΔMDI), with regional mean urban effects (MUEs) reaching up to +36%. In contrast, recently urbanized stations show more heterogeneous responses, with up to 50% demonstrating drought mitigation effects—particularly at longer timescales (SPEI-12)—with MUE reductions as large as –36%. These patterns suggest that modern urban design, green infrastructure, and adaptive planning in newer developments may help alleviate some drought risks. The findings emphasize the importance of accounting for urbanization timing and land-use history when assessing climate risks and planning for urban resilience. Sustainable urban planning and water balance-sensitive design are essential for addressing the multifaceted challenges of urban-induced drought under ongoing climate change and population growth.

Droughts have become one of the world's deadliest and costliest hazards, imposing far-reaching impacts on global agricultural production and sustainable development[1–3]. Recent decades have witnessed intensifying droughts globally[4] including China[5–7], a region highly sensitive to and significantly impacted by global climate change. Since the implementation of afforestation policies in China in 1999, vegetation coverage has increased significantly[8,9]. However, rapid economic development and substantial population growth are constraining the expansion of vegetated areas, leading to vegetation degradation in peri-urban regions. This degradation contributes to increased land surface temperatures, higher potential evapotranspiration (PET), and reduced actual evapotranspiration (ET),

potentially intensifying local drought risks and amplifying the impacts of climate change in urbanized regions[10–13].

China, located within the East Eurasian monsoon zone, is highly vulnerable to frequent and severe droughts[14–16]. These droughts have far-reaching impacts on the country's extensive agricultural systems and broader economic activities, posing significant risks to socio-economic stability[17–19]. Historical records highlight the widespread nature and devastating effects of these drought events. During 1962–1963 and 2010–2011, for example, drought conditions affected more than half of China's non-arid regions[20,21]. More recently, the summer of 2022 brought an extreme drought to eastern China, resulting in substantial economic losses. Similarly, southwest China has experienced several severe drought episodes,

[1]Key Laboratory of the Ministry of Education for Coastal and Wetland Ecosystems, College of Environment and Ecology, Xiamen University, Xiamen, Fujian, China. [2]School of Geographical Sciences, Nanjing University of Information Science and Technology, Nanjing, China. [3]College of Hydrology and Water Resources, Hohai University, Nanjing, China. [4]Leibniz Centre for Agricultural Landscape Research (ZALF), Muncheberg, Germany. [5]Institute of CropScience and Resource Conservation, University of Bonn, Bonn, Germany. [6]Institute for Climate and Application Research (ICAR), Nanjing University of Information Science and Technology, Nanjing, Jiangsu Province, China. ✉e-mail: karam.alsafadi@xmu.edu.cn; wzcao@xmu.edu.cn

with profound impacts on socio-economic conditions, ecosystem functionality, and crops productivity[22–24].

One particularly notable event was the 2006 drought, during which 0.31 million hectares of crops failed, approximately 18 million people faced water shortages, and economic losses reached 11.74 billion yuan[25]. Another devastating drought occurred from late 2009 to early 2010, leaving more than 16 million people and 11 million livestock without adequate drinking water and causing direct economic losses of 19 billion yuan[26,27]. The following year, the 2011 summer drought impacted 5.86 million hectares of crops, leaving 12 million people and 9.17 million livestock without sufficient water[22]. These extreme drought events underscore the ongoing challenges to agriculture, water resources, and ecosystems in China[18,28–30].

Droughts manifest in four primary forms: meteorological, agricultural, hydrological, and socioeconomic[31,32]. These drought types interact with each other. Meteorological droughts, often initiating drought sequences leading to hydrological drought as precipitation deficits persist[33–36]. "Drought Exacerbation" refers to the intensification of drought conditions over time. It implies a trend or pattern where drought events become more severe, in terms of duration, intensity, or spatial extent. Drought exacerbation it often means an analyzing of how drought conditions have become more pronounced with attention to the external drivers compared to historical or baseline observations[37–39]. Factors like global warming and atmospheric circulation changes contribute to precipitation decline, exacerbating drought severity[40–42]. Anthropogenic climate change is widely recognized as a key driver behind the rise in abrupt drought events in China, with greenhouse gas emissions primarily influencing the frequency of flash droughts in simulations[5,43–46]. By 2020, the urbanization rate reached 64%, a significant increase from 18% in 1978, representing a 3.6-fold rise, where the current expansion pace is roughly 20 million individuals annually[47]. Since the 1980s, China's rapid urbanization[48,49] has prompted significant concerns about its potential impact on local drought conditions[50], especially given the extensive urban expansion in the Anthropocene[51,52]. While some studies have proposed a possible link between urbanization and local drought onset[50,53–56], definitive quantitative evidence from historical observational records in China remains lacking.

Significant research has focused on how urbanization affects atmospheric water blance and weather patterns. The Clausius–Clapeyron principle indicates that for every 1 °C rise in temperature, the atmosphere's water vapor capacity increases by approximately 6–7%[57]. This relationship helps to explain the increase in extreme rainfall and flooding in a warming climate. Urban areas, dominated by heat-absorbing surfaces such as asphalt, concrete, and densely built environments, experience significantly higher temperatures compared to their surrounding rural or suburban regions—a phenomenon known as the urban heat island (UHI) effect[58–60]. This effect arises from reduced vegetation, limited actual evapotranspiration, and increased anthropogenic heat emissions, leading to altered local energy balances and enhanced surface and near-surface temperatures[61,62]. This warming is linked to changes in rainfall patterns, with studies showing increased heavy rainfall in cities[63,64]. The UHI can disrupt the boundary layer, affecting atmospheric circulation and promoting localized convection, further exacerbating extreme precipitation[65,66]. Additionally, urbanization alters surface humidity levels compared to rural regions, often reducing urban actual evapotranspiration due to decreased vegetation. Huang et al.[50] highlighted the significant influence of urbanization on rainfall patterns during the rainy season across five major urban regions in China. Their findings indicated that urbanization contributed to increased heavy rainfall by 30.8 to 42.7% while also accounting for a 30.6% reduction in light precipitation. However, in polluted atmospheres in urban areas, aerosols can alter cloud microphysics, extending rainfall durations or intensifying precipitation during specific events[67–69]. Simulations by Shao et al.[70] showed that these aerosols intensify heavy precipitation but reduce moderate and light precipitation.

Considering these dynamics, we propose that urbanization likely significantly impacts local meteorological drought conditions. However, the current understanding of drought causes predominantly highlights large-scale influences at regional and global levels, alongside various climate

patterns. In contrast, the specific local and regional impacts of urbanization on drought duration, severity, and intensity remain insufficiently explored. For instance, Huang et al.[71] investigated the global rise in droughts linked to urbanization, finding that approximately 36% of weather monitoring stations worldwide reported increased drought severity and about 43% of urban areas noted a rise in the extreme Standardized Precipitation Evapotranspiration Index (SPEI). In a regional analysis, Huang et al.[50] employed high-resolution datasets to evaluate the effects of urbanization on local drought in 52 major cities within the Yangtze River Basin (YRB) in China. Their findings indicated that urbanization significantly exacerbated extreme SPEI and drought severity in 69.2% and 61.5% of these cities, respectively. Nonetheless, a substantial gap remains in our understanding of how urbanization may worsen or mitigate local drought conditions in China, particularly when assessed through long-term observational datasets.

The objectives of this study are to examine the drought dynamics across China, with particular emphasis on how both global climate change and urbanization contribute to changes in drought duration, severity, frequency, and intensity. A central aim is to analyze the spatial and temporal differences in drought characteristics between urban and rural areas, using long-term observational data and robust statistical methods. More specifically, the study also aims to quantify the impact of urbanization on drought trends and quantify the influence of urbanization timing—distinguishing between early-urbanized (pre-1985) and recently urbanized (post-1985) areas—on various drought metrics across multiple timescales (SPEI-3, -6, -9, and -12). As part of this, it seeks to explore urbanization's dual role in exacerbating and mitigating drought conditions. Differentiate the effects of urbanization from large-scale climatic forcings, using a comparative approach between urban and rural station pairs to isolate urbanization's specific impact on drought trends and its characteristics. The analyses are performed based on comprehensive historical datasets and advanced statistical methods. Ultimately, the study aims to enhance understanding of how urban development influences hydrometeorological extremes and to inform sustainable urban planning and water management strategies that bolster climate resilience in rapidly urbanizing regions.

Results
SPEI/SPI trends and warming effects in China
The the Mann-Kendall (MK) test was employed to analyze temporal trends in SPEI values (Fig. 1e–h) and compare them with Standardized Precipitation Index (SPI) values derived solely from precipitation data. The trend analysis of SPEI across different time scales (SPEI-3, SPEI-6, SPEI-9, and SPEI-12) revealed that 43.9%, 55.3%, 61.9%, and 64.3% of stations, respectively, exhibited significant negative trends ($P < 0.05$). Conversely, positive trends were identified in 5.3%, 11%, 19%, and 23.6% of the stations for the same time scales. Meanwhile, the SPI trends (Fig. 1a–d) for these time scales indicated significant negative trends in 13.7%, 14%, 14.3%, and 14.6% of the stations, whereas 38%, 40%, 40.3%, and 41.4% of stations showed significant positive trends ($P < 0.05$).

Notably, the patterns of change for SPEI values displayed sharper declines at longer time scales, reflecting annual variations in hydrological wet-dry conditions. Figure 1e–h illustrates that the magnitude of change, represented by the Theil-Sen (TS) slope per decade, shows a declining trend (< -0.1 per decade) near the Hu-Huanyong Line. In contrast, upward trends ($> +0.1$ per decade) are apparent in the northwest, the Qinghai–Tibet Plateau, and southeastern China. Regions like Beijing, Tianjin, Liaoning, Henan, and Shandong exhibit a predominantly negative trend, whereas northeastern Qinghai–Tibet Plateau and eastern Xinjiang have the highest positive Sen's slope values.

For SPI-12, the trends across mainland China are predominantly upward, with a smaller proportion of areas showing a downward trend. Upward trends tend to have greater magnitude, while downward trends are generally less pronounced. SPEI-12 trends, however, display more widespread downward shifts than SPI trends, particularly in northern regions beyond the Qinling–Huaihe Line and provinces such as Yunnan, Sichuan, and Chongqing.
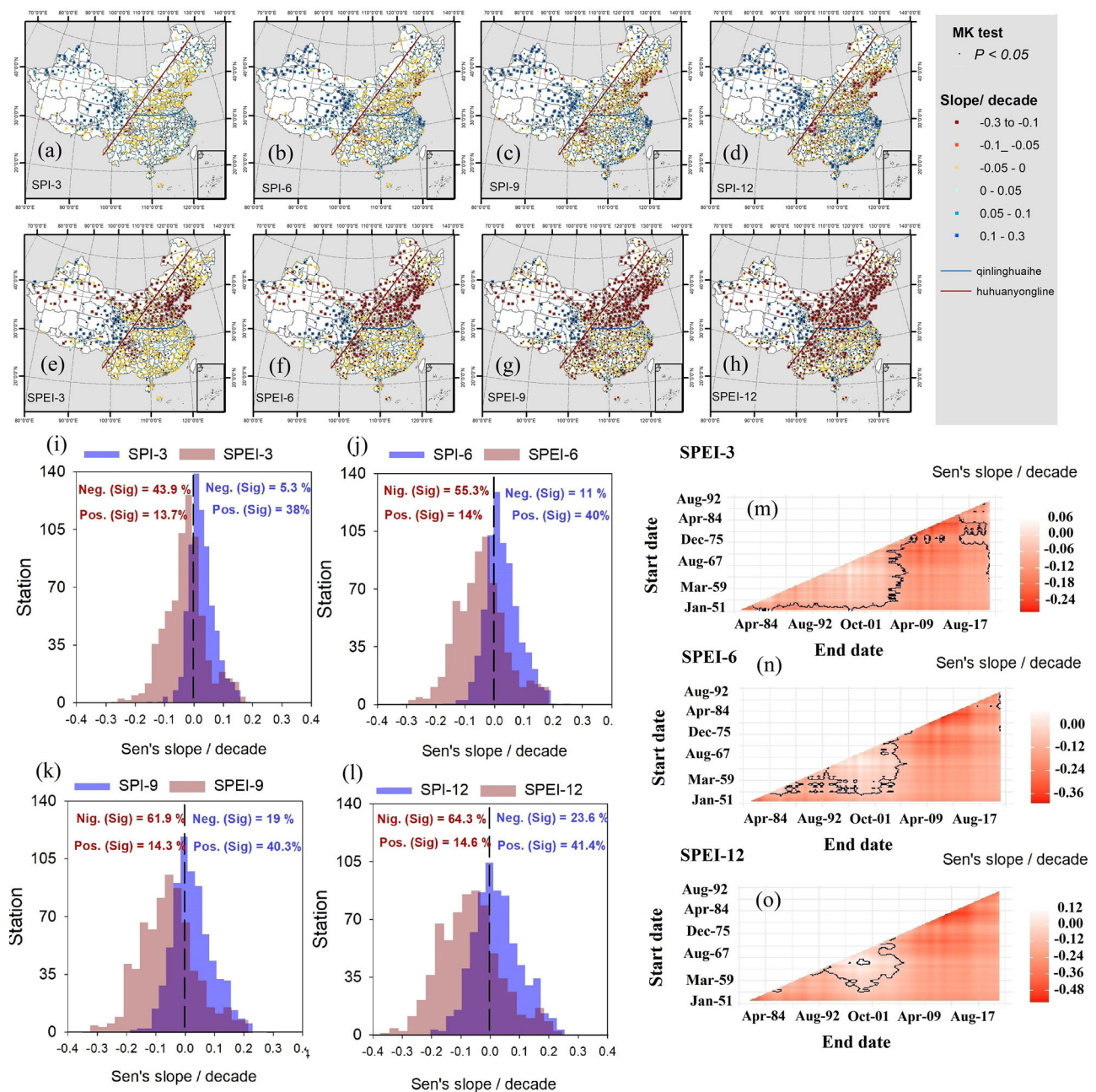
Fig. 1 | Spatial and temporal trends of drought indices (SPI and SPEI) across China (1951–2020). a–d Trends of SPEI at 3-, 6-, 9-, and 12-month timescales. e–h Trends of SPI at the corresponding timescales. Trends were analyzed using the Mann–Kendall (MK) test (P < 0.05) and Theil–Sen (TS) slope estimator per decade. i–l Histograms of the TS slope for SPEI compared with SPI at each timescale, showing the percentage of stations with significant negative (Neg. Sig.) or positive (Pos. Sig.) trends. m–o Heat maps showing regional variations in SPEI trends (based on Supplementary Fig. 1) across multiple temporal windows of 30 years or longer. The magnitude of the trend per decade is expressed as the TS slope, with statistical significance determined by the MK test. Symbols: blue and red dots on maps represent positive and negative trends, respectively; black dot indicates significant slope magnitude.

Regions exhibiting significant upward trends include the northeastern Qinghai–Tibet Plateau, aligning with SPI observations. On the other hand, areas with notable downward trends include southern Xinjiang, western Inner Mongolia, Beijing, Tianjin, southern Liaoning, and eastern Shandong. Interestingly, the trends of SPI and SPEI diverge in regions like south Xinjiang and western Inner Mongolia, while they align in Beijing, Tianjin, southern Liaoning, and eastern Shandong.

The statistical analysis demonstrates substantial spatial-temporal variability in SPEI patterns across mainland China. The SPEI12 time series generally exhibit stable trends, with a more distinct and pronounced decreasing tendency in magnitude and direction, particularly over extended analysis periods. The most significant negative trends were identified in the SPEI12 data during the 1951–2020 period (Supplementary Fig. 1). However, the consistency of these trends across temporal windows exceeding 30 years remains uncertain. Heatmaps illustrating trends across various temporal windows (Fig. 1m–o) for the regional SPEI series show that significant decreases are prevalent across most periods analyzed. A more pronounced decline is evident in recent decades, such as the 1980–2010 window, where over 80% of the windows indicate statistically significant negative trends. These findings suggest that regional warming significantly influences on SPEI trends over time, underscoring the intricate interaction of factors shaping these variations.
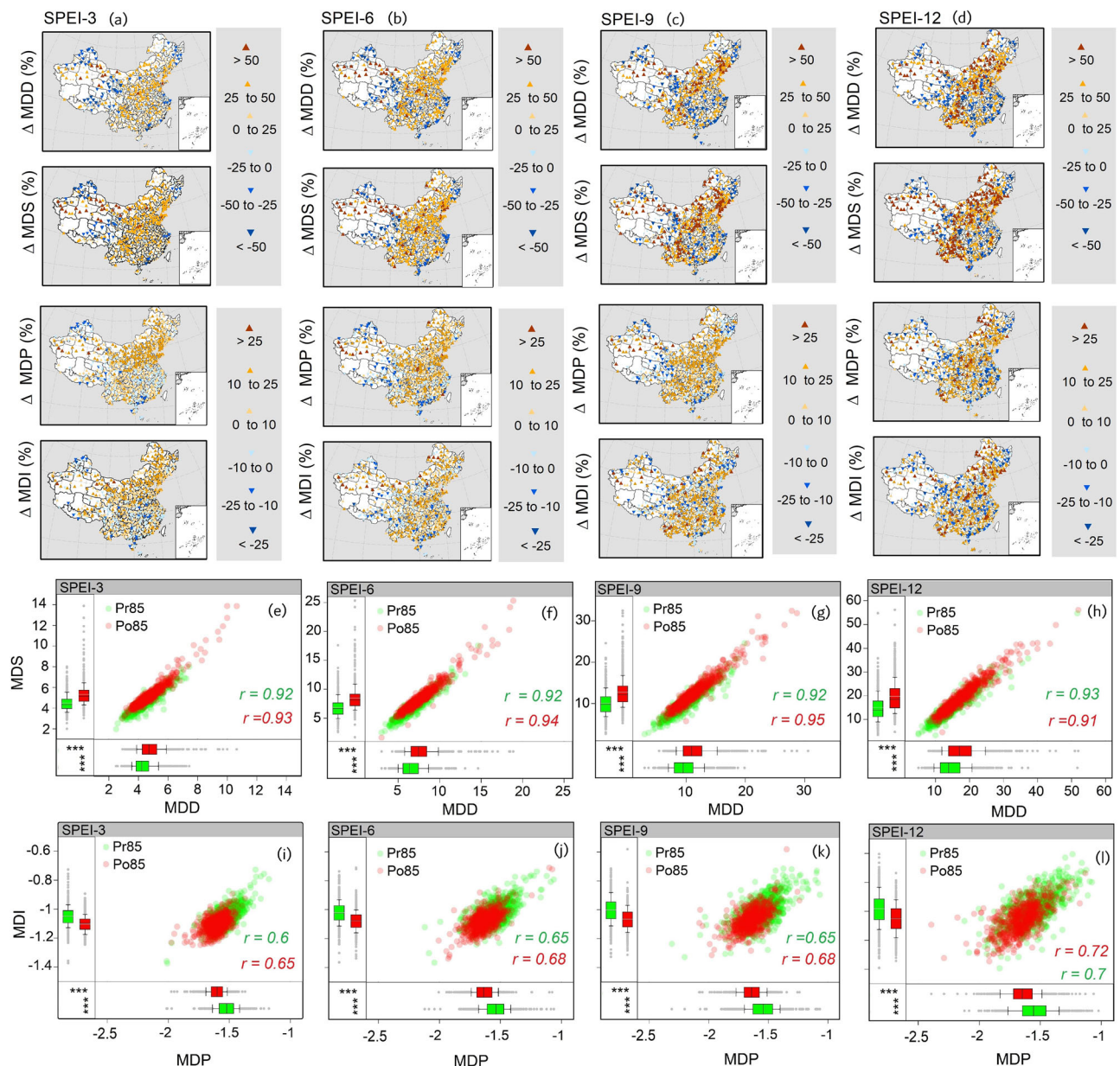
Fig. 2 | Percentage changes in drought attributes before and after 1985 across multiple timescales. a–d Spatial patterns of percentage changes (%) in mean drought duration (ΔMDD), severity (ΔMDS), peak (ΔMDP), and intensity (ΔMDI) between the post-1985 (Po85) and pre-1985 (Pr85) periods, calculated at SPEI-3, -6, -9, and -12 timescales. Positive values indicate an increase in drought attributes after 1985, while negative values indicate a decrease. **e–h** Scatter plots of MDS versus MDD for Po85 and Pr85, with Pearson correlation coefficients (r) displayed for each timescale. **i–l** Scatter plots of MDI versus MDP for Po85 and Pr85, with corresponding correlation coefficients. Box plots beneath each scatter plot summarize the distribution of drought attributes, and statistical differences between periods were tested using Welch's t-test (***P 0.001).

Changes in drought characteristics (ΔDC) reflect the effects of warming

To assess the impact of warming on ΔDC, changes in drought attribute values—including MDCpo85 and MDCpr85 (representing drought attributes for the post-1985 and pre-1985 periods)—were analyzed. These attributes encompass the total number of drought events (TND) and calculate the mean drought duration (MDD), mean drought severity (MDS), mean drought intensity (MDI), and mean peak value (MDP), calculated across various SPEI time scales (SPEI-3, -6, -9, and -12) (Fig. 2). The results revealed that most drought attribute values (ΔDC) changes were positive, while a few areas exhibited negative changes. These negative changes were primarily concentrated in the northwest, northeast, the Qinghai–Tibet Plateau, and southeastern China. Notably, the patterns of change magnitude (%) in drought duration and severity (ΔMDD and ΔMDS) displayed

sharper increases at longer time scales (SPEI-12), reflecting annual variations in hydrological drought conditions. Figure 2 shows that the magnitude of change (%), represented by the difference between the post-1985 and pre-1985 periods, indicates upward trends (>50%) near the Hu-Huanyong Line. Regions such as Beijing, Tianjin, Liaoning, Henan, and Shandong predominantly exhibit increasing changes, and provinces such as Yunnan, Sichuan, and Chongqing are also experiencing increasing changes. In contrast, northeastern Qinghai–Tibet Plateau and eastern Xinjiang show the highest positive values. In contrast, negative ΔMDD and ΔMDS values are evident in the northwest, the Qinghai–Tibet Plateau, and southeastern China.

Similarly, the magnitude of changes (%) in drought intensity and peak (ΔMDI and ΔMDP) showed moderate increases across various time scales, aligning to some extent with changes in other drought attribute values.
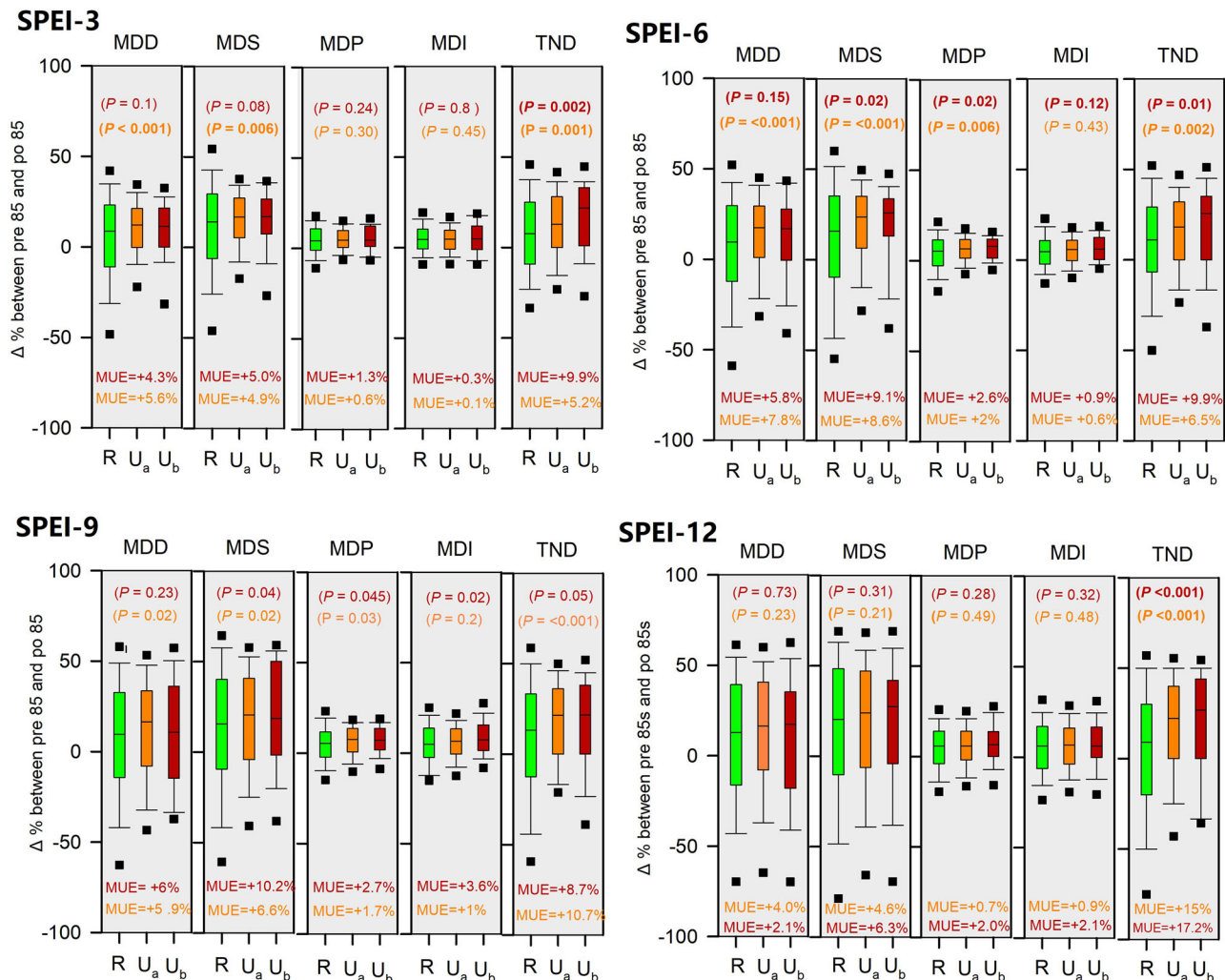
Fig. 3 | Regional impacts of urbanization on drought characteristics across different timescales. Box plots show differences in percentage changes (Δ%) of drought metrics between rural (R) and urban stations (U$_a$: urbanized after 1985 or recently urbanized areas; U$_b$: urbanized before 1985, see Supplementary Fig. 4). Drought attributes include mean drought duration (MDD), severity (MDS), peak (MDP), intensity (MDI), and total number of droughts (TND), evaluated at SPEI-3, -6, -9,

and -12 timescales. ΔDC values were calculated as the difference between post-1985 (MDCpo85) and pre-1985 (MDCpr85) periods. Statistical significance was tested using Welch's t-test (P-values shown above each panel). Mean urban effects (MUE), expressed as the average difference in drought attributes between urban and rural stations, are reported in each panel.

These results highlight upward changes (10–25%) in regions east of the Hu-Huanyong Line.

To evaluate the regional impact of warming on DC metrics across all stations, we compared MDCpo85 and MDCpr85 (representing drought attributes for the post-1985 and pre-1985 periods) using the Welch's t-test. A statistically significant difference (***P < 0.001) confirmed that global warming had intensified drought conditions (Fig. 2, shown through scatter plots). The results revealed significant positive changes and shifts in DC metrics between MDCpo85 and MDCpr85 across China (***P < 0.001) at all timescales. Additionally, MDD and MDS exhibited a strong correlation in both periods.

Observed evidence of changes in drought dynamics due to urbanization

To assess the regional impact of urbanization on ΔDC, we examined differences in ΔDC metrics between urban and rural areas using the Welch's t-test. A negative and statistically significant difference (P < 0.05) indicated that urbanization intensified drought conditions, while a positive and significant result (P < 0.05) suggested that urbanization mitigated drought (Fig. 3). When no significant difference was observed, urbanization was considered to have no discernible impact on drought dynamics.

The analysis showed that ΔMDD differences between station urbanized after 1985 and rural stations were significant (P < 0.05) at shorter time scales, particularly SPEI-3 and SPEI-6, with regional MUEs of +5.6% and +7.8%, respectively, indicating that urbanization intensified drought duration. Similarly, In SPEI-6 (semiannual scale), significant urbanization effects are observed, particularly in ΔMDS. Both categories of urban stations —U$_a$ (urbanized after 1985) and U$_b$ (urbanized before 1985)—exhibit higher then ΔMDS compared to rural stations, with MUE of +8.6% and +9.1%, respectively. Significant differences (P < 0.05) in ΔMDP were observed for both categories of urban stations compared to rural stations at SPEI-6 and SPEI-9. Although most ΔDC metrics did not exhibit substantial differences across all comparisons based on Welch's t-test statistics, these results indicate subtle yet meaningful changes that can be attributed to urbanization effects.

Notably, ΔTND differences between both urban station categories and rural stations were statistically significant (P < 0.05) across all SPEI timescales. The regional MUE for ΔTND in U$_a$ stations (urbanized after 1985) was +5.2%, +6.5%, +10.7%, and +15.0% for SPEI-3, SPEI-6, SPEI-9, and SPEI-12, respectively. For U$_b$ stations (urbanized before 1985), the corresponding MUE values were +9.9%, +9.9%, +8.7%, and +17.2%. These results underscore that urbanization consistently increases the frequency of
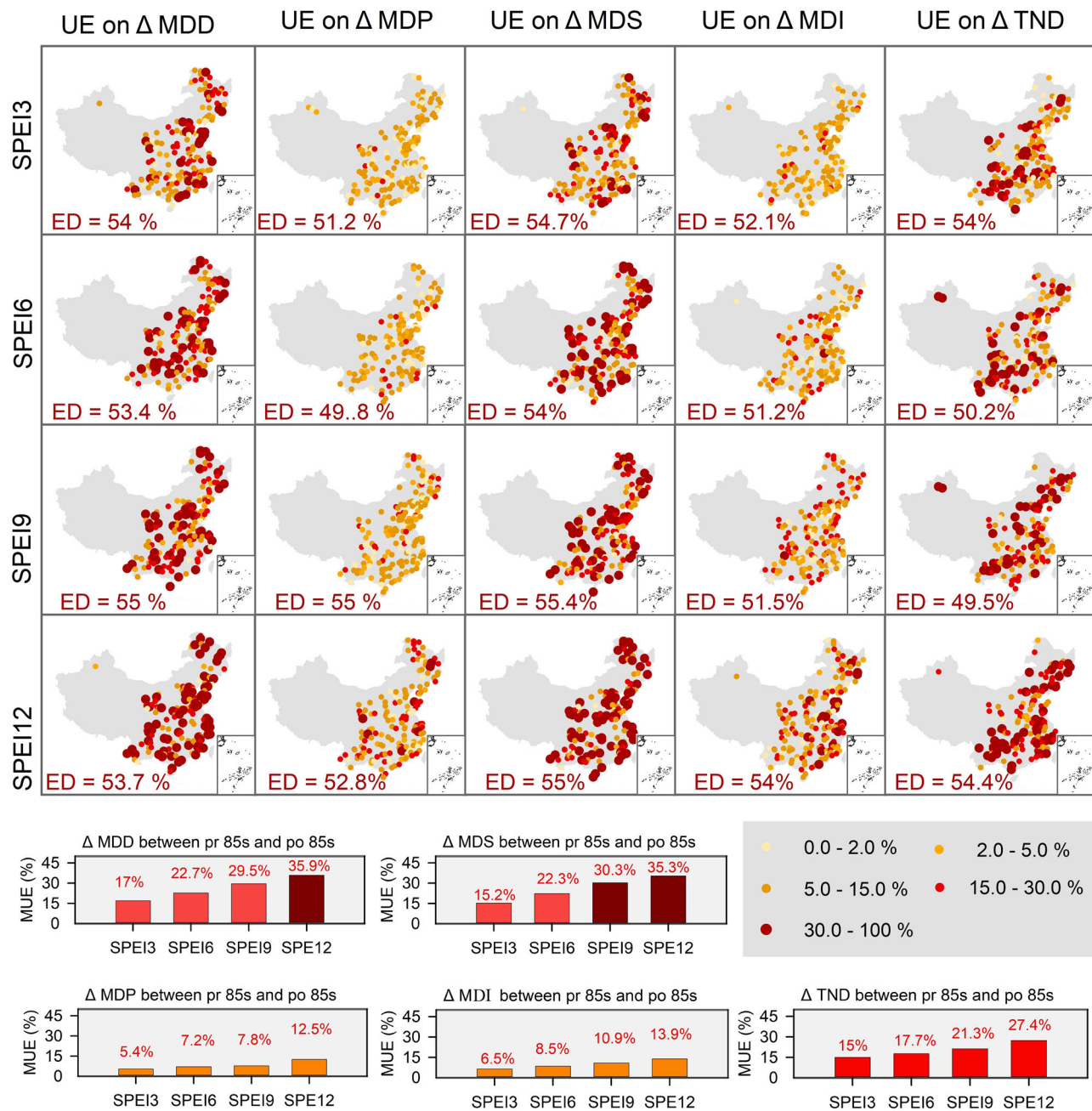
Fig. 4 | Spatial distribution of urbanization effects on drought characteristics in China. Urbanization effects (%UE) on changes in drought characteristics (ΔDC) were evaluated across four SPEI timescales (SPEI-3, SPEI-6, SPEI-9, SPEI-12) by comparing drought metrics between urban (ΔDCUi) and rural (ΔDCRi) station pairs (Eq. 9). Maps display the spatial distribution of %UE for five drought metrics: mean drought duration (MDD), mean drought peak (MDP), mean drought severity (MDS), mean drought intensity (MDI), and total number of droughts (TND). Color and symbol coding indicate the magnitude of effects. ED refers to "exacerbated drought" conditions, where urbanization contributed to intensifying drought severity. The analysis includes stations that transitioned from rural to urban after 1985 (Ua, urbanized after 1985), underscoring the role of recent urban expansion (1985–2020) in amplifying drought intensity. Bottom panels summarize mean urbanization effects (MUE, %) on ΔDC between the pre-1985 and post-1985 periods, illustrating systematic increases in drought characteristics associated with urbanization.

drought events, regardless of the time scale. And underscore the complex and multifaceted ways urbanization influences drought dynamics, varying across different drought metrics and timescales.

To investigate the impact of urbanization on local drought conditions, meteorological stations were classified as urban or rural based on 2020 land-use data, which reflect the extent of urban expansion between 1985 and 2020. This approach allowed the identification of stations that transitioned from rural to urban during this period (U$_a$: urbanized after 1985). The analysis revealed that 44% of the stations (309 cities) were classified as urban

(Supplementary Fig. 4). As a key step, the urban effects on changes in drought characteristics (UE on ΔDC) were assessed by analyzing differences in drought characteristics between urban and rural station pairs (Eq. 9). The results (Fig. 4) showed that approximately 50–55% of urban stations exhibited exacerbation of drought (ED) dynamics for UE on ΔΔMDD, ΔMDP, ΔMDS, ΔTND, and ΔMDI. For instance, the MUE on ΔMDD increased from +17% at SPEI-3 to +35.9% at SPEI-12, while the MUE on ΔMDS ranged from +15.2% to +35.3% across the same timescales. However, 45–50% of the urban stations (U$_a$) demonstrated drought mitigation
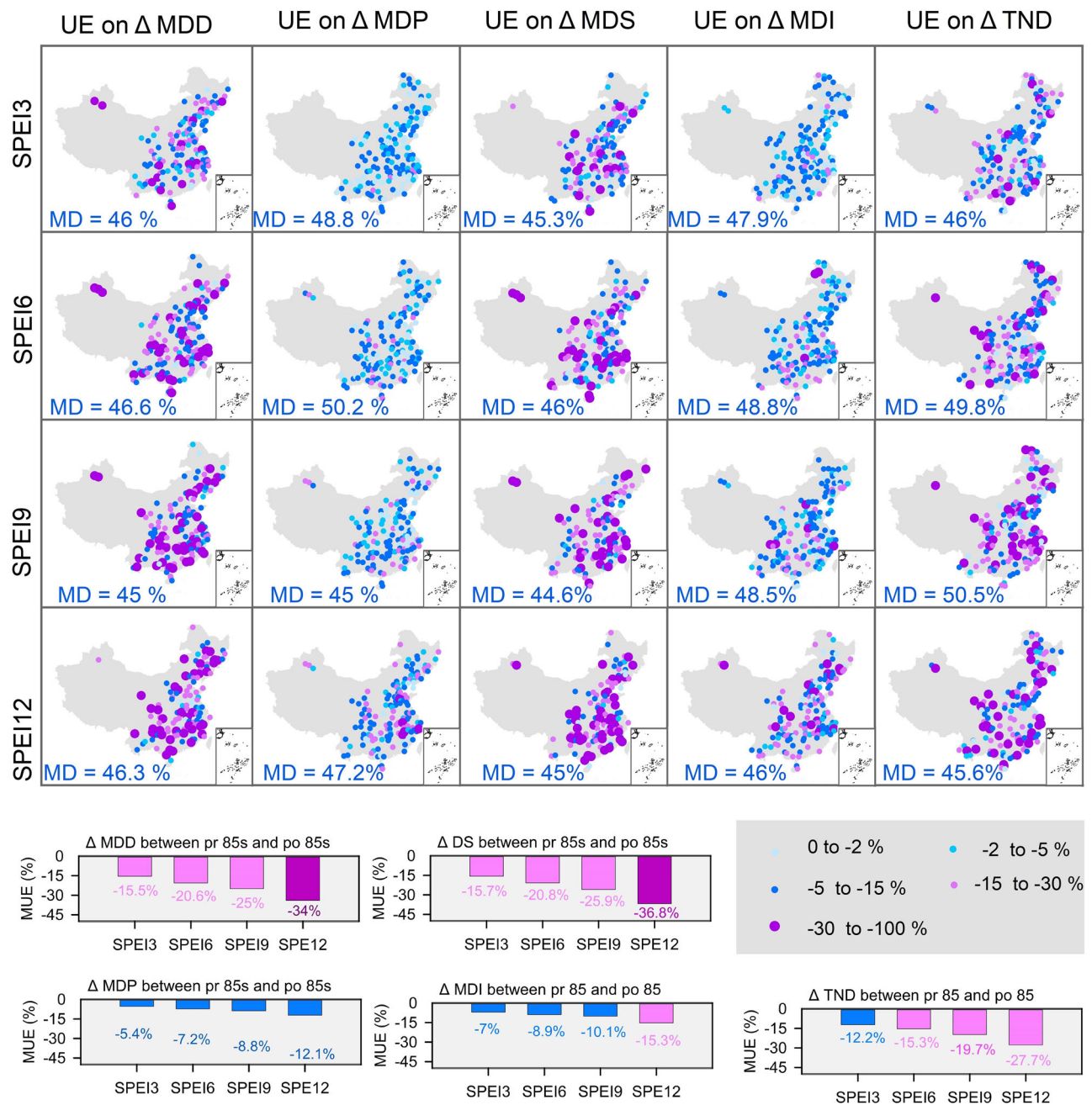
Fig. 5 | Spatial distribution of urbanization effects on drought characteristics in China. Urbanization effects (%UE) on changes in drought characteristics (ΔDC) were evaluated across multiple SPEI timescales (SPEI-3, SPEI-6, SPEI-9, SPEI-12) and quantified by comparing drought metrics between urban (ΔDCUi) and rural (ΔDCRi) station pairs (Eq. 9). Maps show the spatial distribution of %UE for five drought metrics: mean drought duration (MDD), mean drought peak (MDP), mean drought severity (MDS), mean drought intensity (MDI), and total number of droughts (TND). Color and symbol coding indicate the magnitude and direction of urbanization effects. MD refers to "mitigating drought" conditions, where urbanization contributed to reduced drought severity. The analysis includes stations that transitioned from rural to urban after 1985 (U_a, urbanized after 1985), highlighting the role of recenturban expansion (1985–2020) in amplifying drought intensity. Bottom panels present mean urbanization effects (MUE, %) on ΔDC between the pre-1985 and post-1985 periods, emphasizing systematic changes in drought characteristics linked to urban growth.

(MD), especially for longer timescales. Specifically, the MUE for ΔMDD declined from –15.5% to –34% and for ΔMDS from –15.7% to –36.38% between SPEI-3 and SPEI-12. Similarly, MUEs for ΔMDP and ΔMDI ranged from –5.4% to –12.1% and –7% to –15.3%, respectively. Mitigation of ΔTND was also evident among U_a stations, with MUE ranging from –12.2% to –27.7% across SPEI-3 to SPEI-12 (Fig. 5).

On the other hand, stations were also classified using 1985 land-use data to identify those already urbanized before 1985 (U_b: urbanized before 1985), enabling an assessment of early-urbanized areas and their impact on drought dynamics. This classification identified only 6.9% of stations (48 cities) as urban by 1985 (Supplementary Fig. 4). The UE on ΔDC was evaluated similarly by comparing urban (U_b) and rural station pairs (Eq. 9).

The results presented in Fig. 6 offer a more nuanced understanding of how urbanization influences drought characteristics across different timescales. Both drought exacerbation (ED) and mitigation (MD) effects were evident across all drought metrics (ΔMDD, ΔMDP, ΔMDS, ΔMDI, and ΔTND), though the overall distribution was more balanced than previously reported. At shorter timescales (e.g., SPEI-3), the urbanization effect on
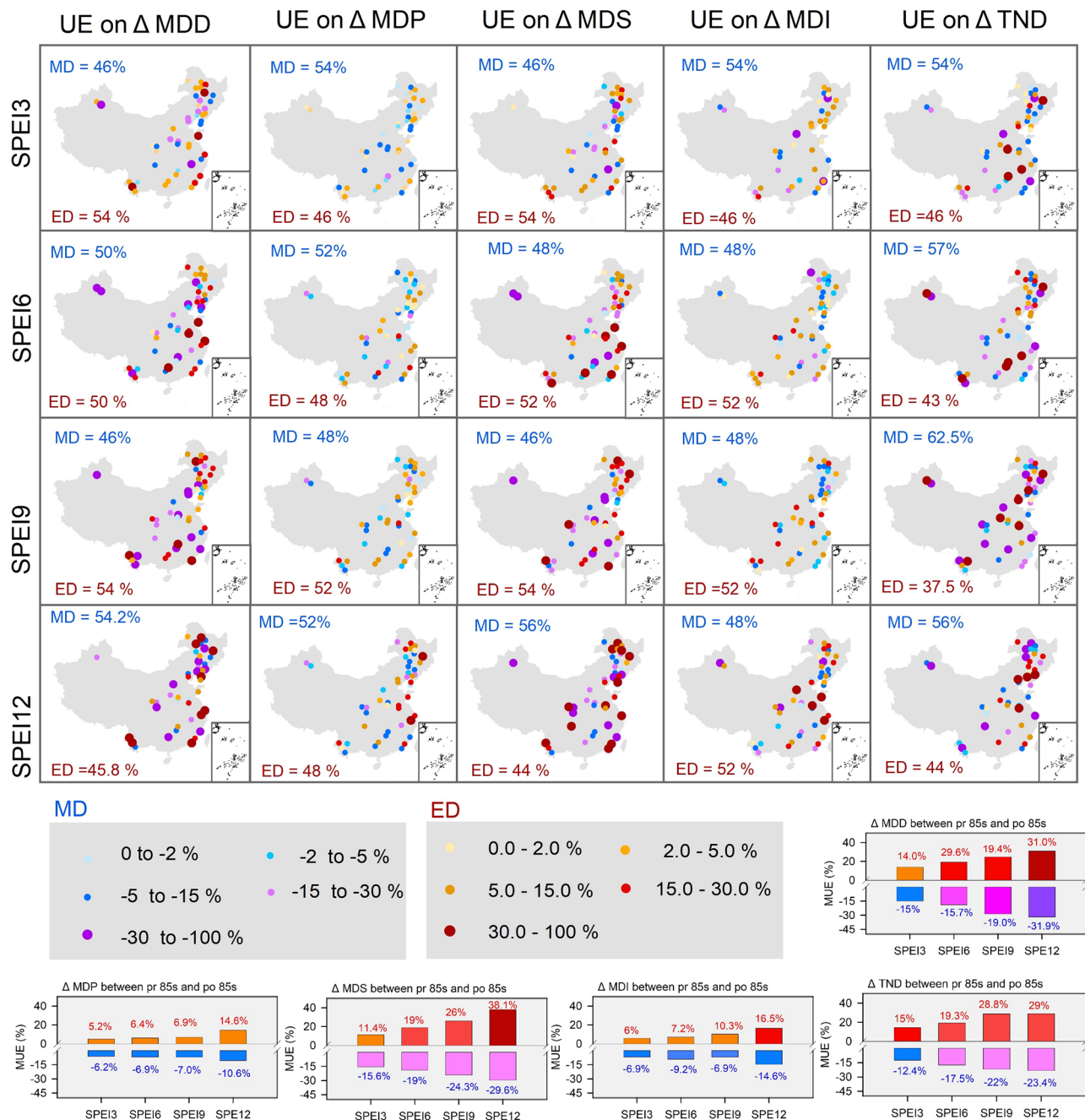
Fig. 6 | Spatial distribution of urbanization effects on drought characteristics in China. Urbanization effects (%UE) on changes in drought characteristics (ΔDC) were evaluated across multiple SPEI timescales (SPEI-3, SPEI-6, SPEI-9, SPEI-12) and quantified by comparing drought metrics between urban (ΔDCUi) and rural (ΔDCRi) station pairs (Eq. 9). Maps illustrate the spatial distribution of %UE for five drought metrics: mean drought duration (MDD), mean drought peak (MDP), mean drought severity (MDS), mean drought intensity (MDI), and total number of droughts (TND). Color and symbol coding represent the magnitude and direction of urbanization effects. MD and ED denote "mitigating drought" and "exacerbated drought" conditions, where urbanization contributed to reducing or intensifying drought severity, respectively. The analysis includes stations that transitioned from rural to urban before 1985 (U$_b$, urbanized before 1985). Bottom panels summarize mean urbanization effects (MUE, %) on ΔDC between the pre-1985 and post-1985 periods, highlighting systematic positive and negative changes in drought characteristics associated with urban growth.

ΔMDD and ΔMDS was nearly evenly split between ED and MD (54% vs. 46%), while drought mitigation effects were slightly more prevalent for ΔTND, ΔMDP, and ΔMDI, with 54–57% of stations showing reduced drought severity. As the timescale lengthened, mitigation effects became more dominant for certain metrics. For example, at SPEI-12, 56% of stations exhibited MD for both ΔMDS and ΔTND, while the effects on ΔMDD and ΔMDI remained more evenly distributed. Notably, ΔMDI showed consistent mitigation proportions (~48%) across all timescales, suggesting a complex and potentially offsetting relationship between urbanization and drought intensity. The MUE further illustrates this dual role. In long-urbanized areas (stations urbanized before 1985, U$_b$), MUE for ΔMDD increased from +14.0% at SPEI-3 to +31.0% at SPEI-12, indicating a stronger drought-exacerbating influence with increasing drought accumulation period. Similar exacerbation patterns were observed for ΔMDS (rising from +11.4% to +38.1%) and ΔTND (from +15.0% to +29.0%), highlighting the intensified impact of legacy urbanization on longer-term
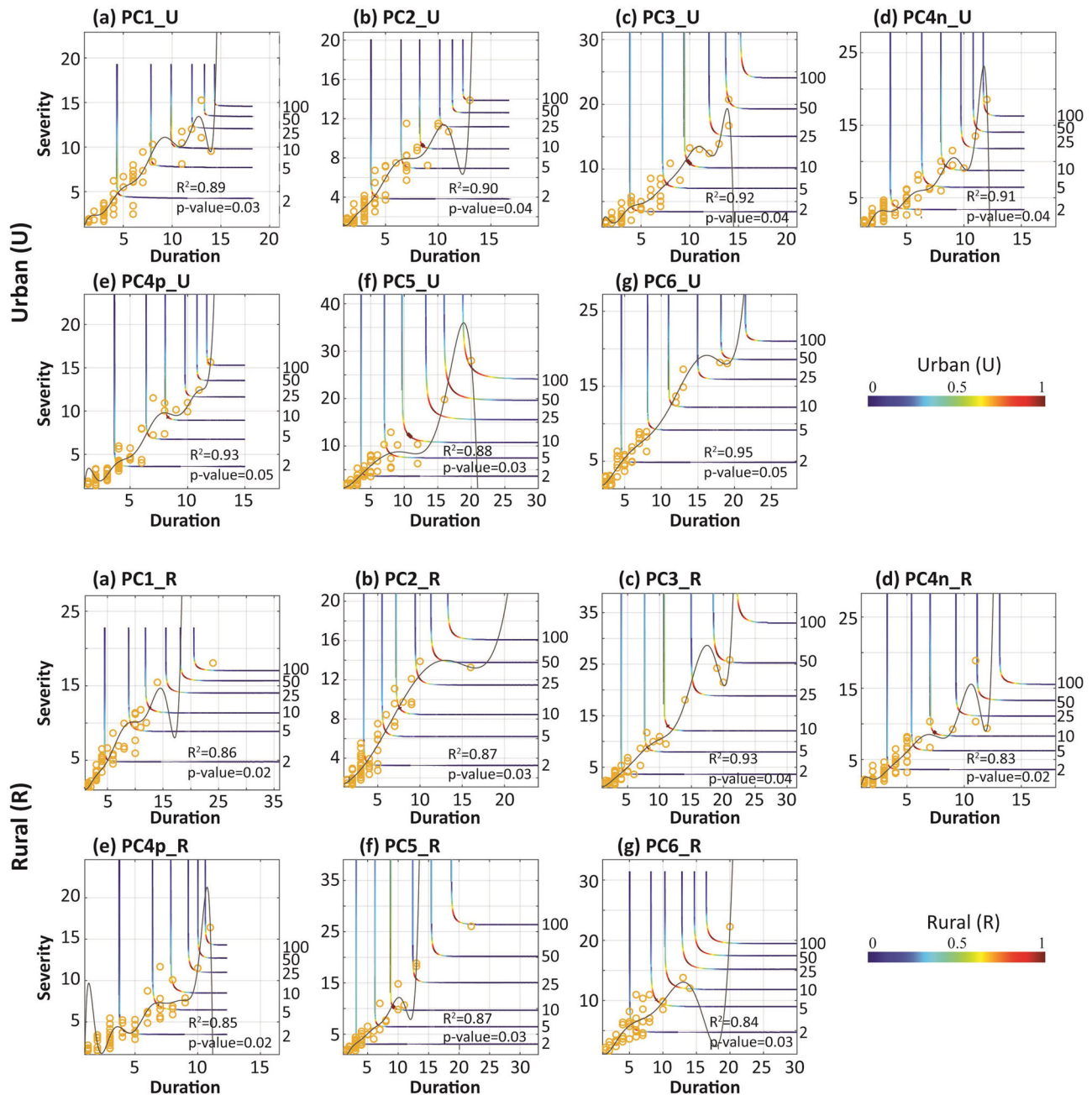
Fig. 7 | Bivariate drought probabilities and joint return periods (JRPs) of drought risk for urban and rural stations, defined by drought duration and severity, are presented to demonstrate the intervals between drought events under varying climate patterns in China. Climate patterns of SPEI were derived using PCA (Supplementary Figs. 2 and 3). Based on SPEI-3, the analysis applied bivariate copulas and OR-based return periods (Tor) to evaluate drought events from 1951 to 2020.

drought metrics. In contrast, recently urbanized stations (urbanized after 1985, U_a) displayed more pronounced drought mitigation. MUE for ΔMDD ranged from –15.5% to –34.0%, while Ub stations showed slightly less pronounced reductions (–15.0% to –31.9%). Comparable mitigation trends were observed for ΔMDS (–15.7% to –36.8% in U_a vs. –15.6% to –29.6% in Ub), ΔMDI (–7.0% to –15.3% in U_a vs. –6.9% to –14.6% in U_b), and ΔMDP (–4.5% to –12.1% in Ua vs. –6.2% to –10.6% in U_b). These patterns suggest that more recent urban development may benefit from climate-resilient infrastructure or increased occurrence of localized convective rainfall events, helping to offset the adverse effects of urbanization on drought severity.

Furthermore, we used Joint return period (JRP) of drought to characterize drought frequency risk, representing the time intervals between drought events under different climate patterns in China, classified using

PCA (Supplementary Figs. 2 and 3). The drought return period was calculated based on the joint distribution of DD and DS, modeled using a copula function (see Methods section). Given the strong correlation between drought duration and severity, we observed that some urban stations exhibit shorter return periods then to their rural counterparts (Fig. 7), particularly for PC2 and PC5, representing Shanghai and Kunming, respectively.

For instance, the urban station in Shanghai (PC2) recorded only four TND events with JRP ≥ 10 years, compared to six events at its paired rural station. Similarly, the Kunming (PC5) urban station recorded only two TND events with JRP ≥ 10 years, compared to five events at its paired rural station. These findings suggest that urban stations in PC2 and PC5 are at an increased risk of experiencing prolonged and severe drought events of a given magnitude and intensity, with shorter return periods. Conversely,

some urban stations exhibit longer return periods than their rural counterparts (Fig. 7), particularly for PC1, PC4p, and PC6, representing Beijing, Nanjing, and Urumqi, respectively. For example, the urban station in Beijing (PC1) recorded five TND events with JRP ≥ 10 years, compared to only two events at its paired rural station. These findings indicate that urban stations in PC1, PC4p, and PC6 are at a reduced risk of experiencing prolonged and severe drought events of a given magnitude and intensity, with longer return periods. Refer to Supplementary Table 1 and Supplementary Fig. 5 for more detailed drought frequency results.

Discussion

The inconsistency between SPI and SPEI trends reflects the influence of warming effects

The observed inconsistency between SPI and SPEI trends underscores the influence of warming on drought dynamics across mainland China. While SPI—based solely on precipitation—often shows widespread positive trends, SPEI trends are predominantly negative, especially at longer time scales (SPEI-6, SPEI-9, and SPEI-12). This divergence highlights the critical role of temperature-driven increases in evapotranspiration, which are captured by SPEI but overlooked by SPI.

The MK test results reveal substantial spatial and temporal variability in SPEI trends, reflecting the complex interplay between climatic warming, precipitation variability, and hydrological drought. Across all time scales, a higher proportion of negative SPEI trends indicates intensifying drought conditions as warming exacerbates atmospheric water demand. This is particularly evident in regions such as northern China, Yunnan, Sichuan, and Chongqing, where downward SPEI trends contrast with neutral or even positive SPI trends.

The stronger decline in SPEI-12 compared to SPI-12, especially in areas north of the Qinling–Huaihe Line, provides compelling evidence that warming amplifies water deficits over longer periods. This supports findings by Alsafadi et al.[72] and Sun et al.[55], who emphasized the increasing role of evaporative demand in driving hydrological drought under climate change. Theil-Sen's slope (TS) analysis further reinforces this pattern, showing spatially divergent SPEI trends. Significant declines are concentrated near the Hu–Huanyong Line, including major urban centers such as Beijing, Tianjin, and Shandong, where rapid urbanization and associated climatic stress likely exacerbate drought conditions. In contrast, regions such as the northwestern arid zones, the Qinghai–Tibet Plateau, and parts of southeastern China exhibit positive SPEI trends this supports findings by Wang et al.[73], potentially due to localized hydrological resilience or differing climate drivers. While this research suggests a potential link between urbanization and the onset or intensification of local droughts, definitive quantitative evidence from long-term observational records in China remains limited. The contrasting trends in early-urbanized versus recently urbanized regions imply that urbanization may play a dual role—either intensifying or mitigating drought—depending on regional climatic, hydrological, and land-use contexts. This duality will be further investigated in the following sections through detailed analyses of urban effects on drought characteristics.

The heatmaps (Fig. 1m–o) offer further temporal resolution, showing how the direction and intensity of trends vary across different start–end time windows. For SPEI-12, the heatmap reveals persistent and intensifying negative trends, particularly in windows beginning in the 1980s and extending into the 2010s, where over 80% of the time windows exhibit statistically significant declines. This period coincides with the accelerated warming phase in China, reinforcing the interpretation that temperature-driven evapotranspiration is a dominant force behind the observed drying trends. In contrast, SPEI-3 and SPEI-6 display less pronounced and more variable trends, indicating that short-term drought patterns are more influenced by precipitation variability and less sensitive to evapotranspiration effects. This temporal contrast emphasizes that longer accumulation periods (e.g., SPEI-12) are more effective for capturing the cumulative hydrological impacts of warming, making them essential for drought monitoring and climate adaptation planning. Overall, these results

underscore that regional warming has not only intensified drought severity but also altered its temporal persistence and spatial expression, especially over extended periods and in northern and urbanized regions of China. This highlights the need for long-term, temperature-sensitive drought indices like SPEI-12 in future climate impact assessments.

Changes in drought characteristics and the effects of warming

The analysis of changes in drought characteristics (ΔDC), particularly the differences between post-1985 (MDCpo85) and pre-1985 (MDCpr85) periods, provides further insights into the effects of warming. The observed increases in drought duration (ΔMDD) and severity (ΔMDS) at longer time scales, such as SPEI-12, indicate that warming-driven changes in hydrological cycles are intensifying drought conditions across much of China[74]. Regions near the Hu-Huanyong Line, as well as Yunnan, Sichuan, and Chongqing, show significant upward changes in drought attributes, consistent with broader climatic warming trends. These findings are corroborated by studies which similarly identify contrasting trends in extreme drought events between eastern and western China[75–77]. This observation is consistent with the findings of Liang et al.[75], who identified contrasting patterns in extreme drought events: cities east of the Hu-Huanyong Line exhibit upward trends, while those west of the line demonstrate downward trends.

The interplay between UHI effects and urban microclimates in arid regions creates phenomena such as Urban Wet Islands (UWI), where localized rainfall can diminish drought impacts relative to surrounding rural areas. Urban zones often experience intense and sporadic precipitation events driven by anthropogenic aerosols, which act as cloud condensation nuclei (CCN). These aerosols foster cloud formation and rainfall during warm rain[78–80]. However, in polluted atmospheres, aerosols can alter cloud microphysics, extending rainfall durations or intensifying precipitation during specific events[67,81–83]. This intricate dynamic often leads to fragmented precipitation patterns that reduce the frequency and severity of prolonged droughts in some urban areas. Interestingly, the magnitude of change in drought intensity (ΔMDI) and peak (ΔMDP) demonstrates moderate increases across various time scales, suggesting that while drought events are becoming more frequent and prolonged, their intensity is not increasing as sharply. This particular observation highlights the importance of evaluating multiple metrics to capture the full complexity of drought dynamics under warming scenarios.

On the other hand, urbanization can exacerbate drought conditions in certain cities. Replacing vegetated areas with impervious surfaces reduces evapotranspiration and the availability of local atmospheric moisture, contributing to the development of Urban Dry Islands (UDI)[84,85]. This reduction in vegetative cover diminishes latent heat flux (LE), impairs water vapor exchange and evapotranspiration[50]. Impervious surfaces also alter soil heat capacity and reduce infiltration rates, increasing sensible heat flux (H)[86,87]. These combined effects elevate vapor pressure deficits (VPD), increase potential evapotranspiration (PET), and reduce relative humidity (RH), creating drier urban environments and reinforcing drought conditions (see Fig. 8). The higher VPD suppresses light rainfall (LP) and sustains droughts.

The statistically significant differences in MDC metrics (***P < 0.001) between pre- and post-1985 periods confirm the role of global warming in amplifying drought conditions. The strong correlation between MDD and MDS across both periods further suggests a consistent linkage between drought duration and severity, reinforcing the hypothesis that warming-induced evapotranspiration is a key driver of these changes.

Urbanization and its impact on drought dynamics

Urbanization exerts a complex and dual influence on meteorological drought dynamics, impacting its duration, intensity, and frequency across urban areas[54]. While it may mitigate drought conditions in some cities, it can exacerbate them in others, depending on interactions among climate, land-surface dynamics, and anthropogenic factors[50]. In urban environments, impervious surfaces such as asphalt and concrete replace natural vegetation,
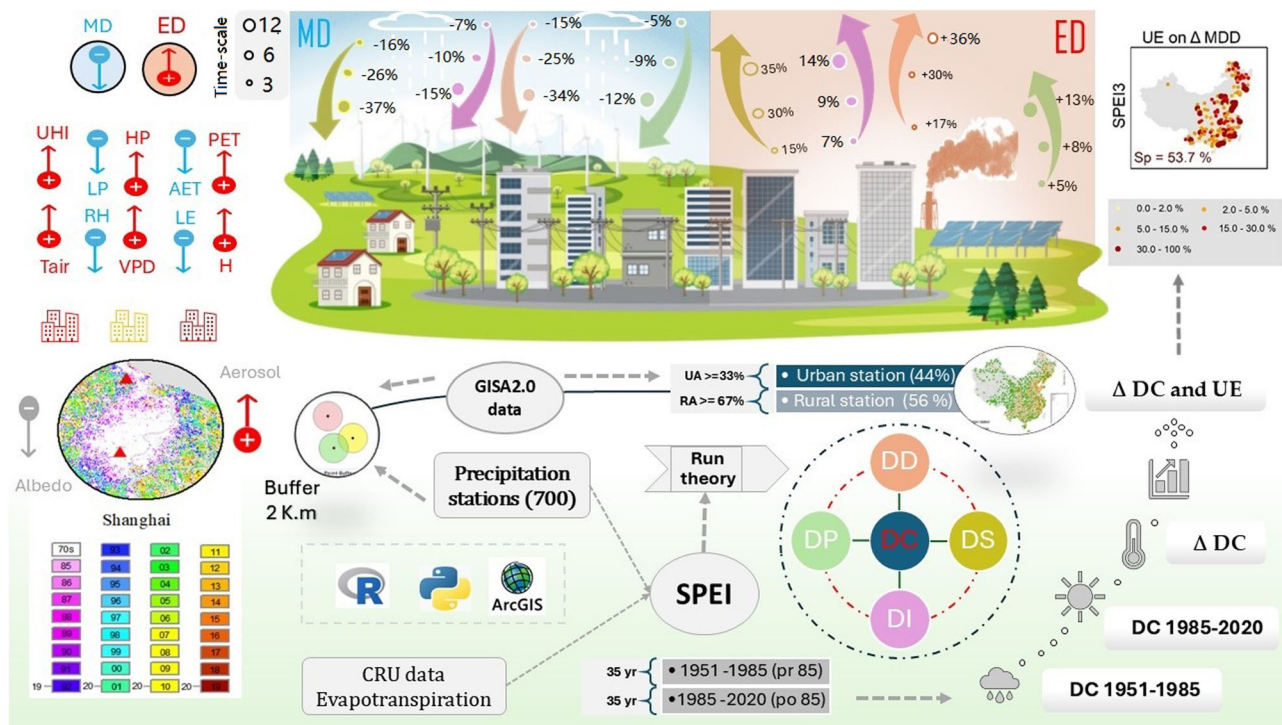
Fig. 8 | Schematic representation of urbanization's dual role in exacerbation and mitigation of drought (ED and MD) dynamics. The figure illustrates the dual role of urbanization in exacerbating and mitigating drought dynamics (ED and MD) using SPEI data from 700 stations across China from 1951–2020. The flowchart in the lower section outlines the characterization of drought (DC) events based on their duration (DD), severity (DS), intensity (DI), and peak (DP). It also depicts the calculation of drought characteristics (ΔDC) changes between two periods (pre-1985 and post-1985). Subsequently, urban effects (UE) on ΔDC were analyzed to identify changes in drought characteristics for urban-rural paired stations. Notes: Tair Air temperature, LP Light precipitation, HP Heavy precipitation, RH Relative humidity, PET Potential evapotranspiration, AET Actual evapotranspiration, VPD: Vapor pressure deficit, H Sensible heat flux, LE Latent heat flux, UHI Urban heat island. Note: The visual elements of the figure were created using vector assets from Vectorpocket (Freepik.com) and ArcGIS 10.8, while additional components were designed using Microsoft PowerPoint.

limiting water infiltration, increasing surface runoff, and disrupting natural water cycles and energy balances[88,89]. Furthermore, heat emissions from industrial processes, transportation, and dense infrastructure contribute to localized warming, commonly referred to as the UHI effect[90]. This localized warming alters wind circulation patterns, enhances convection, and facilitates the formation of convective clouds like cumulonimbus, which can produce heavy rainfall[91–93]. In this context, Liang et al.[75] observed that extreme rainfall events in most Chinese cities exhibit increasing trends specifically in eastern China. Additionally, UHI-induced warming can channel moisture-laden air into cities, leading to localized rain events that partially alleviate drought severity and duration.

The results also reveal the multifaceted influence of urbanization on drought dynamics. The Welch's t-test indicates that urbanization has both exacerbating and mitigating effects, depending on the specific drought metric and region. For shorter time scales (SPEI-3 and SPEI-6), urbanization appears to intensify MDD and MDS, with regional MUE of +4% to +9% (Fig. 3.). This intensification is likely due to UHI effects, which enhance evapotranspiration and reduce soil moisture availability in urbanized areas.

Conversely, the results show that urbanization mitigates drought conditions in approximately 45–50% of urban stations, particularly at longer time scales (SPEI-9 and SPEI-12). This mitigation may be attributed to improved water management and infrastructure in urban areas, which could buffer against prolonged drought impacts. The observed reductions in MDP and in ΔMDI in some urban areas support this hypothesis.

The increase in the frequency of drought events (i.e., TND) in urban stations, despite urbanization intensifying the duration and severity of drought, can be attributed to several interrelated factors. One primary reason is fragmented precipitation patterns caused by anthropogenic aerosols and pollution, which alter cloud microphysics, suppress light rainfall, and create localized disruptions in precipitation[94,95]. These factors lead to intermittent and fragmented rain events that fail to mitigate drought conditions effectively. On the other hand, the UHI effect intensifies localized warming, fostering conditions favorable for short-lived convective precipitation events. While these events may briefly interrupt prolonged drought periods, they typically do not supply enough moisture to alleviate the overall drought duration and severity, instead resetting the drought cycle more frequently. Urban areas also exhibit a heightened sensitivity to water balance deficits due to altered atmospheric hydrology and higher evaporative demand. This increased sensitivity makes urban areas more vulnerable to short-term water balance deficits, rapidly classified as drought events, contributing to a higher recorded frequency of droughts.

Aerosols, categorized as anthropogenic and natural (e.g., mineral dust), significantly influence precipitation, with effects varying by intensity. Anthropogenic aerosols often suppress precipitation in northern China while enhancing it in southern China[96,97]. Simulations by Shao et al.[70] showed that these aerosols intensify heavy precipitation by 70.96% but reduce moderate and light precipitation by 24.87% and 86.43%, respectively. Their effects also vary diurnally, suppressing daytime precipitation by stabilizing the atmosphere and reducing convection but enhancing nocturnal convection and extreme precipitation[98].

Mineral dust aerosols, recognized as CCN and ice-nucleating particles (INP), also exhibit dual roles in precipitation. They suppress weak precipitation but intensify heavy rainfall by activating mixed-phase clouds and forming ice crystals[99]. For instance, dust aerosols significantly increase convective clouds and torrential rain[100]. Regional studies highlight varied responses: in the Himalayas, dust enhances heavy precipitation in higher terrains[101], while in the Sierra Nevada and the Red Sea, dust modulates precipitation differently based on elevation and synoptic conditions[102].

Urbanization timing and its role in changing drought dynamics

The timing of urbanization has emerged as a critical factor in changing local drought dynamics, a finding that aligns with and extends the growing body of literature on urban climate impacts. In this study, we found that early-urbanized stations (U_b) are consistently associated with exacerbated drought conditions, particularly evident in short-term drought frequency (ΔTND) and severity indices (ΔMDS and ΔMDI). This is reflected in the high proportion of urban stations exhibiting exacerbation of drought (ED) and in the positive values of the MUE. In contrast, recently urbanized stations (U_a) demonstrated a more heterogeneous response, with many stations showing drought mitigation (MD), particularly at longer timescales such as SPEI-12. These contrasting patterns underscore the significance of urbanization history in modulating local hydroclimatic conditions.

The findings for U_b stations are consistent with earlier studies that attribute intensified drought risk in older urban cores to long-term land-use legacies, including increased impervious surfaces, suppressed evapotranspiration, and altered surface energy balances[103,104]. For example, Huang et al.[71] demonstrated that nearly 40% of cities globally experienced worsened extreme drought conditions due to sustained urban expansion, particularly in regions where green infrastructure was historically limited. These findings are mirrored in our results, where urbanization prior to 1985 (U_b) led to clear and consistent increases in drought severity and frequency across multiple timescales.

Conversely, U_a stations, urbanized after 1985, displayed mixed but often mitigative effects on drought characteristics. Several mechanisms may explain this pattern. Recent urban expansions may have integrated green spaces, water-sensitive urban design, and climate adaptation strategies, which enhance local water retention and reduce surface runoff. Moreover, modern urban forms may induce localized convection through the UHI effect, potentially increasing precipitation frequency and intensity, especially in short-duration events[105]. For instance, studies in rapidly growing Chinese cities like Urumqi have shown that UHI-driven convective rainfall can offset drought tendencies in newly urbanized zones[106] This supports the observed drought mitigation trends in U_a stations, particularly for ΔMDD and ΔMDS (See PC6 results in Supplementary Table 1.).

Importantly, short-term drought indices (e.g., SPEI-3 and SPEI-6) were more sensitive to the influence of early urbanization, likely due to the cumulative impacts of impervious surface buildup, altered hydrology, and reduced soil moisture retention over decades. These results emphasize that legacy effects of urban land-use are deeply embedded in the drought response of cities and are not easily reversed.

Furthermore, spatial analysis indicates that urban drought exacerbation is more pronounced in eastern and central China, regions with high urban density and early industrial development. This spatial alignment with long-standing urbanization further supports the idea that historical land-use changes play a more decisive role than mere urban extent in influencing local drought regimes.

Drought frequency risk and joint return period analysis (JRP)

The JRP analysis provideed valuable insights into the risk of prolonged and severe drought events under different climatic patterns. Urban stations, particularly in regions like Shanghai (PC2) and Kunming (PC5), exhibit shorter return periods for drought events compared to their rural counterparts. This increased risk highlights the compounded vulnerability of urban areas to extreme drought conditions, driven by a combination of climatic and anthropogenic factors. Conversely, urban stations in Beijing (PC1), Nanjing (PC4p), and Urumqi (PC6) exhibit longer return periods, suggesting reduced drought frequency risk in these regions. These findings may reflect localized climatic or infrastructural factors that mitigate drought impacts in certain urban areas.

Research Contributions, gaps, and Limitations

This study reveals the complex and spatially heterogeneous nature of drought dynamics across China, driven by the combined influences of regional warming, evolving land-use patterns, and the pace and timing of urbanization. The clear divergence between SPI and SPEI trends underscores the growing importance of temperature-driven evapotranspiration in shaping drought conditions—especially in northern China and other warming-prone regions—highlighting how conventional precipitation-based indices may underestimate drought risk under climate change. Urbanization is identified as a critical modifier of local drought characteristics, with its effects varying based on historical context and development trajectories. Stations urbanized before 1985 (U_b) consistently exhibit more severe and frequent short-term droughts, as shown by high ΔTND, ΔMDS, and ΔMDI values and predominantly positive MUEs. In contrast, more recently urbanized areas (U_a) often display mixed responses, with many showing signs of drought mitigation—particularly at longer timescales—likely due to improved urban planning practices, integration of green infrastructure, and adaptive climate responses in newer developments.

These findings reinforce the importance of urbanization timing in assessing drought vulnerability and resilience. Historical land-use legacies in early-urbanized regions continue to amplify drought risks, while recent urban growth presents opportunities to implement more climate-resilient designs. In terms of policy and adaptation, the results emphasize the need for time-sensitive and spatially tailored urban planning strategies. Integrating green infrastructure—such as vegetated surfaces, permeable pavements, and rainwater harvesting systems—can help alleviate the urban heat island effect and mitigate drought impacts. Additionally, promoting water-efficient technologies and irrigation practices, particularly in agricultural regions vulnerable to warming-induced water stress, is vital. Incentivizing drought-resistant crops and improving irrigation efficiency in northeastern China are practical steps toward enhancing water security. Ultimately, this research provides actionable insights for policymakers, urban planners, and climate resilience stakeholders, offering a pathway toward more adaptive and sustainable urban development in the face of accelerating climate change.

This study helps bridge this gap through several key contributions: (i) It utilizes dynamic, high-resolution land-use data (GISAv.3.0) to classify meteorological stations based on urbanization timing (i.e., pre-1985 vs. 1985–2020), enabling a temporally nuanced analysis of urbanization's effects. (ii) It applies a spatial pairing approach between urban and rural stations, controlling for elevation and proximity, which helps isolate urbanization-specific impacts from broader regional climate trends. (iii) It quantifies urbanization's dual role—both in exacerbating and mitigating drought characteristics—a dimension that is seldom captured within a unified analytical framework. (iv) It offers novel insights into the temporal sensitivity of urban effects on drought indices across different time scales (e.g., SPEI-3 vs. SPEI-12), thus enhancing the temporal resolution and interpretability of urban drought dynamics.

However, we acknowledge several limitations in our approach: (i) Although the stations classified as rural, some stations may still be affected by indirect anthropogenic influences such as agricultural activities or peri-urban expansion. (ii) The assumption that paired rural stations reflect only broad-scale climatic forcings may not always be valid, especially in transitional or semi-developed regions. (iii) The station classification is based on a threshold of 33% impervious surface within a 2 km buffer, which—while consistent with high-resolution land-use standards—may oversimplify the complexity of urban morphology and overlook subtle land-use transitions. (iv) While the urban–rural pairing method helps isolate urbanization effects, the attribution could be further refined through pixel-level land cover transition analysis, particularly in areas with fine-scale spatial heterogeneity or recent rapid development. Despite these limitations, our study contributes methodologically and conceptually by integrating high-resolution spatial data with temporally sensitive trend analysis. This dual-scale framework provides new insights into the multifaceted role of urbanization in modulating drought dynamics and offers valuable guidance for urban planners and climate adaptation strategies.

Methods

Study area and data collection

China, located in the eastern region of the Eurasian continent, spans from approximately 3°51′N to 53°33′N in latitude and 73°33′E to 135°5′E in longitude, covering a vast land area of around 9.6 million square kilometers. Its eastern border meets the Pacific Ocean, while the southwestern border adjoins the Qinghai-Tibet Plateau. These diverse geographical features give rise to distinct climate patterns, categorized as monsoon and continental climates[107,108]. In China, most precipitation is concentrated during the summer across most regions, although its distribution varies. The eastern regions receive higher precipitation levels than the western areas, with a gradual decline in precipitation from the southeast coast to the northwest inland. This phenomenon is attributed to the influence of winter monsoons, which are cold and dry during the winter while summer monsoons originating from the ocean bring warmth and rain and impact during the summer months[109,110].

The extensive eastern region of China is significantly influenced by the southeast and southwest monsoons, resulting in abundant rainfall. In contrast, the inland northwest experiences limited precipitation due to the weaker influence of the summer monsoon (Supplementary Fig. 4). For this study, monthly precipitation data for the period 1951–2016 were collected from the China Meteorological Data Sharing Service System (http://data.cma.cn/en, accessed on 28 February 2018). The dataset included records from 756 benchmark ground observation stations across most parts of the country. However, due to data limitations, 52 stations were excluded.

To address missing data, monthly precipitation records from 1951 to 2020 were obtained from the Global Precipitation Climatology Center[111] (GPCC) (http://gpcc.dwd.de/, accessed on 24 February 2023). These data were used to correct and fill missing values using linear equations, resulting in a final dataset covering 700 stations for the 1951–2020 period (Supplementary Fig. 4). The precipitation data underwent a homogeneity test before being utilized for drought index analysis. Supplementary figures (Supplementary Figs. 5 and 6) provide additional details on the GPCC data's performance in correcting missing values, demonstrating a high correlation with observed precipitation records.

Similarly, evapotranspiration data for the 1951–2020 period were obtained from the Climatic Research Unit's global gridded dataset[112] (CRU TS v4.06) at the University of East Anglia, UK (https://crudata.uea.ac.uk/cru/data/hrg/, accessed on 1 February 2023). SPI/SPEI values calculated over a 3-, 6-, 9-, and 12-month period for the entire study area are presented as a two-dimensional array.

Drought indices calculation

To evaluate the effects of urbanization on local meteorological drought, we utilized the SPEI[113] as the primary metric for assessing drought conditions. Unlike other indices such as the Palmer Drought Severity Index, SPEI offers flexibility througdh its variable timescales, making it suitable for analyzing long-, medium-, and short-term drought events. Urbanization often leads to significant changes in impervious surfaces and vegetation cover, and SPEI's inclusion of evapotranspiration provides a more comprehensive measure of the impact of atmospheric aridity on water resources and ecosystems. SPEI is derived by transforming the water balance (precipitation minus PET) into a log-logistic distribution, a method extensively applied in prior research[24,43,114]. PET was calculated using the FAO-56 Penman-Monteith approach, which was recognized for its accuracy and implemented with data from the CRU TS v4.06 dataset. Additional details regarding the computation of SPEI can be found in Supplementary Note 1.

Temporal patterns (trend analysis, principal components analysis)

To calculate SPEI temporal patterns across China, the MK[115,116] was used. The MK statistical test, recommended by the World Meteorological Organization (WMO) for hydro-climatic data analysis, is widely used as a non-parametric method for analyzing time series. Unlike other tests, the MK test does not require the data to follow a specific distribution. It is commonly applied to identify trends in hydro-meteorological time series, such as rainfall, temperature, and drought indices[72]. The MK test is robust in detecting trends and is unaffected by outliers or non-normal distribution. This study used the MK test to determine statistically significant increasing or decreasing trends in SPEI within a 95% confidence interval ($p < 0.05$) over a specific period. Autocorrelations in time series can influence the results of the MK test, as observed in previous studies[117]. The TS's slope estimator assessed the magnitude and extent of trends in SPI and SPEI time series[118,119]. The TS's slope estimator is a non-parametric method for estimating the slope of a linear regression model. This method is robust to outliers and makes no assumptions about the data distribution. It is particularly useful when dealing with data that contains outliers or when the relationship between variables is not strictly linear. Additional details regarding the TS slope estimator and MK test computation can be found in Supplementary Note 2.

To comprehensively assess SPEI trends across various timescales, we analyzed all possible temporal windows of 30 years or longer within the study period. This method helped evaluate the sensitivity of observed trends (both positive and negative) to variations in the selected timeframe[120]. The findings were represented through heat maps, which showcased the trend magnitude (calculated using TS's slope) alongside statistical significance (determined by the MK test). Considering the large number of observation stations, creating individual heat maps for each was not feasible. Instead, we employed Principal Component Analysis (PCA) in S-mode[121] to condense and identify spatial patterns with similar SPEI trends.

The analysis prioritized SPEI-12 due to its reliability in reflecting long-term trend stability. Six principal components (PCs) were derived from the dataset beginning in 1951, accounting for 46.3% of the total regional SPEI variance. These components exhibited a uniform distribution across mainland China (Supplementary Fig. 1). Each PC was paired with its most correlated station, and the corresponding trends were visualized in the same units as the original SPEI data. This facilitated the depiction of decade-scale changes and trend patterns via heat maps. Analyzing the spatial distributions of the component loadings, we pinpointed the geographic areas most influenced by each trend pattern. This analysis was instrumental in understanding the impact of urbanization on meteorological drought conditions in cities with diverse climates and SPEI characteristics.

Drought identification and characterization

We defined five drought metrics based on SPEI to analyse drought development further. For each station, we identified the thresholds for the onset and termination of drought events across two periods reflecting the indirect effects of urbanization: 1951–1985 and 1985–2020. This analysis utilized Run Theory to determine drought characteristics systematically. The Run theory, proposed by Yevjevich et al.[122], is a widely utilized method for characterizing drought events[123]. In this approach, a run refers to a consecutive period in a time series where all values remain below a specified threshold[124]. This study defines a drought event following McKee et al.[125] as a sequence of negative SPEI values lasting at least one month, with the lowest SPEI value below -1. Characterizing drought events holds significant importance for several reasons. Firstly, prolonged droughts can substantially impact agriculture, vegetation growth, and the local environment[126]. Secondly, identifying drought events starting from negative SPEI values can aid in improving drought early-warning systems. The Run theory allows for the definition and characterization of a drought event based on its duration (DD), severity (DS), intensity (DI), and peak (DP). DD is determined by calculating the number of months between the start and end of the drought. DS is measured as the absolute sum of SPEI/SPI values during drought. DI is obtained by calculating the average SPEI values within the drought duration and dividing it by the duration. DP refers to the lowest SPEI value during the drought peak time.

Drought event indices are calculated using the Run theory at each station to analyse the spatiotemporal characteristics of drought[55]. This allows us to determine the total number of drought events (TND) and calculate the mean drought duration (MDD), mean drought severity

(MDS), mean drought intensity (MDI), and mean peak value (MDP) at each station (Supplementary Fig. 7 based on SPEI data and Supplementary Fig. 8 for SPI data). Identifying the season when droughts are initiated can greatly contribute to regional drought mitigation efforts.

$$MDD = \frac{\sum_{i=1}^{N} DD_i}{N} \quad (1)$$

$$MDS = \frac{\sum_{j=1}^{N} DS_j}{N}, \ DS = \sum_{i}^{DD} |SPEI_i| \quad (2)$$

$$MDI = \frac{\sum_{j=1}^{N} DI_j}{N}, \ DI = \frac{\sum_{i}^{DD} |SPEI_i|}{DD} \quad (3)$$

$$MDP = \frac{\sum_{j=1}^{N} DP_j}{N}, \ DP = \max_{1 \le i \le DD} |SPEI_i| \quad (4)$$

$$\Delta DC(\%) = \frac{MDC_{po85}i - MDC_{pr85}i}{MDC_{po85}i} \times 100 \quad (5)$$

ΔDC is the change value of drought attribute, *MDC po*85 and *MDCpr*85 the are drought attribute post-1985 and pre-1985, including MDD, MDS, MDI, MDP, TND), and MDC is the mean drought characteristics.

Joint return period (JRP) of drought using bivariate copula

To evaluate drought characteristics comprehensively, we integrated drought duration and severity using copula functions[127]. Due to their adaptable marginal distributions, these are highly versatile for modeling interdependent hydrometeorological variables. Joint return periods (JRPs) were calculated for drought events across six distinct SPEI drought patterns identified through PCA over China. This analysis utilized three primary copula families—Gaussian, Frank, and Gumbel—to estimate the joint distribution of drought duration and severity. Among the various return period definitions, such as "OR", "AND", Kendall, and dynamic methods, the OR criterion (T_{or}) was predominantly employed to assess drought occurrence probabilities[128]. The marginal distributions of drought duration and severity were first determined using six statistical distributions: Gamma, Generalized Extreme Value (GEV), Weibull, Normal, Log-normal, and Inverse Gaussian. The best-fitting marginal and copula functions were selected using the Akaike Information Criterion (AIC)[129] and Ordinary Least Squares (OLS). For more details see Supplementary note 3.

Based on Sklar's theorem[127], the joint probability distribution was formulated as $D(d, s) = C(D_D(d), D_s(s))$, where C represents the copula function, and $D_D(d)$ and $D_S(s)$ denote the cumulative distribution functions for drought duration and severity, respectively. Each region's most suitable copula family was identified, allowing for precise estimation of bivariate drought probabilities and JRPs[130,131]. Similarly, the Gaussian, Gumbel, and Frank copulas are ranked as the bivariate suggested distributions:

$$\begin{cases} C_{Gaussian}(\theta) = \Phi_\theta(\Phi^{-1}(D_D), \Phi^{-1}(D_S)), \ \theta \in (-1, 1) \\ C_{Gumbel}(\theta) = \exp\left\{-\left[(-\ln(D_D))^\theta + (-\ln(D_S))^\theta\right]^{\frac{1}{\theta}}\right\}, \ \theta \in [1, \infty) \\ C_{Frank}(\theta) = -\frac{1}{\theta}\ln\left(1 + \frac{(e^{-\theta D_D}-1)(e^{-\theta D_S}-1)}{(e^{-\theta}-1)}\right), \ \theta \in ((-\infty, 0), (0, \infty)) \end{cases} \quad (6)$$

In recent studies employing the copula framework, several methodologies for JRPs have been proposed[132,133]. These include the "OR", "AND", Kendall, and dynamic-based return period approaches[127,131]. Of these, the OR-based return period (T_{or}) is the most commonly applied method, particularly for analyzing the occurrence probabilities of extreme

events such as droughts and floods[134,135] and can be expressed as:

$$T_{or} = \frac{E_l}{1 - F(d, s)} = \frac{E_l}{1 - C[D_D(d), D_S(S)]} \quad (7)$$

E_l represents the inter-arrival time for estimated drought (D) events under the bivariate analysis framework. The calculation of T_{or} is influenced by the wide range of possible combinations of drought events. Its determination can be achieved using the following mathematical formulation[136]:

$$\begin{cases} (d^*, s\$^*) = argmax D(d, s) = C[D_D(d), D_S(S)]f_D(d), f_S(S) \\ C(D_D(d), D_S(S)) = 1 - E_l/T_{or} \end{cases} \quad (8)$$

The joint distribution of drought events, denoted as D(d, s), is described by the copula function, $C[D_D(d), D_S(S)] = dC\frac{(d), D_S(S)}{d(D_D(d))}$, $d(D_D(d))$ represents the copula density function, while $f_D(d) and f_S(S)$ correspond to the probability density functions for drought duration $D_D(d)$ and drought severity $D_S(S)$, respectively.

This approach offered significant insights into the spatial and temporal patterns of drought intensification, providing a comprehensive framework to evaluate the combined impacts of drought duration and severity under diverse climatic conditions across China. The variation in JRP between urban and rural station pairs was utilized to quantify the influence of urbanization on drought frequency.

Assessing the impact of urbanization on local drought

To investigate the impact of urbanization on local drought conditions, meteorological stations were classified as either urban or rural based on land-use data from 1985 and 2020, which capture patterns of urban expansion. Stations were categorized according to whether they transitioned from rural to urban prior to 1985 (urbanized before 1985) or during the period 1985–2020 (urbanized after 1985). This classification utilized dynamic GISA v.3.0 impervious surface areas (ISA) data[137], where circular buffers were generated around each station to calculate the proportion of impervious surface area. Stations with impervious surface fractions exceeding a predetermined threshold were classified as urban, while those below the threshold were designated as rural[138–140] (Supplementary Fig. 4).

In this study, a buffer radius of 2 km and an impervious surface threshold of 33% were applied, consistent with best practices for 30 m resolution land-use data. These parameters align with prior research, which typically uses a 7 km radius with a 20% threshold for 1 km resolution data and a 2 km radius with a 33% threshold for high-resolution datasets[50,71,103,141].

To account for regional variability, each urban station was paired with its nearest rural counterpart within a 100 km radius[138,139]. Rural stations with an elevation difference exceeding 500 m from the urban station were excluded to minimize topographic influences[71]. Drought metrics for each urban-rural pair were analyzed, with differences attributed to the effects of urbanization.

The urbanization effect (UE) was quantified by examining changes in drought characteristics (ΔDC) between two periods (pre-1985 and post-1985). The UE on ΔDC was applied to identify these changes in DC for urban-rural pairs stations, providing a robust measure of urbanization's role in shaping local drought dynamics (Fig. 8).

$$UE(\%) = \Delta DC_{Ui} - \Delta DC_{Ri} \quad (9)$$

Where ΔDC_{Ui} and ΔDC_{Ri} represent changes in drought attributes for for urban-rural pairs stations, respectively. And $\Delta DC(\%)$ can be calculated based on (Eq. 5). Thus, the difference in the change of drought characteristics between urban and rural stations ($\Delta DC_{Ui} - \Delta DC_{Ri}$) is interpreted as the UE, with the rural trend acting as a baseline for broader climate-driven changes. To assess the statistical significance of differences in ΔDC between urban and rural stations, we applied Welch's t-test For more details see Supplementary note 4.

Codes availability

Data availability

References

1. Jaeger, W. K. et al. Scope and limitations of drought management within complex human–natural systems. *Nat. Sustain.* **2**, 710–717 (2019).
2. Christian, J. I. et al. Global distribution, trends, and drivers of flash drought occurrence. *Nat. Commun.* **12**, 6330 (2021).
3. Wang, G. et al. Exogenous moisture deficit fuels drought risks across China. *npj Clim. Atmos. Sci.* **6**, 217 (2023).
4. Rohde, M. M. Floods and droughts are intensifying globally. *Nat. Water* **1**, 226–227 (2023).
5. Yuan, X. et al. Anthropogenic shift towards higher risk of flash drought over China. *Nat. Commun.* **10**, 4661 (2019).
6. Omer, A., Zhuguo, M., Zheng, Z. & Saleem, F. Natural and anthropogenic influences on the recent droughts in Yellow River Basin, China. *Sci. Total Environ.* **704**, 135428 (2020).
7. Chen, D. et al. Contribution of anthropogenic influence to the 2022-like Yangtze River valley compound heatwave and drought event. *npj Clim. Atmos. Sci.* **7**, 172 (2024).
8. Ge, W., Deng, L., Wang, F. & Han, J. Quantifying the contributions of human activities and climate change to vegetation net primary productivity dynamics in China from 2001 to 2016. *Sci. Total Environ.* **773**, 145648 (2021).
9. Zhou, Y., Fu, D., Lu, C., Xu, X. & Tang, Q. Positive effects of ecological restoration policies on the vegetation dynamics in a typical ecologically vulnerable area of China. *Ecol. Eng.* **159**, 106087 (2021).
10. Alsafadi, K. et al. An evapotranspiration deficit-based drought index to detect variability of terrestrial carbon productivity in the Middle East. *Environ. Res. Lett.* **17**, 014051 (2022).
11. Wu, B. et al. Mitigation of urban heat island in China (2000–2020) through vegetation-induced cooling. *Sustain. Cities Soc.* **112**, 105599 (2024).
12. Yao, R. et al. Urbanization effects on vegetation and surface urban heat islands in China's Yangtze River Basin. *Remote Sens* **9**, 540 (2017).
13. Wang, Z. et al. Enhanced evapotranspiration induced by vegetation restoration may pose water resource risks under climate change in the Yellow River Basin. *Ecol. Indic.* **162**, 112060 (2024).
14. Shen, C., Wang, W. C., Hao, Z. & Gong, W. Exceptional drought events over eastern China during the last five centuries. *Clim. Change* **85**, 453–471 (2007).
15. Zhang, Q., Xiao, M. & Singh, V. P. Uncertainty evaluation of copula analysis of hydrological droughts in the East River basin, China. *Glob. Planet. Change* **129**, 1–9 (2015).
16. Zhang, R. et al. A stratospheric precursor of East Asian summer droughts and floods. *Nat. Commun.* **15**, 247 (2024).
17. Zhao, Z. & Wang, K. Capability of existing drought indices in reflecting agricultural drought in China. *J. Geophys. Res. Biogeosciences* **126**, e2020JG006064 (2021).
18. Li, P. et al. Various maize yield losses and their dynamics triggered by drought thresholds based on Copula-Bayesian conditional probabilities. *Agric. Water Manag.* **261**, 107391 (2022).
19. Mokhtar, A. et al. Assessment of the effects of spatiotemporal characteristics of drought on crop yields in southwest China. *Int. J. Climatol.* **42**, 3056-3075 (2022).
20. Jia, J. et al. Drought risk analysis of maize under climate change based on natural disaster system theory in Southwest China. *Shengtai Xuebao* **36**, 340–349 (2016).
21. Xu, K. et al. Spatio-temporal variation of drought in China during 1961-2012: a climatic perspective. *J. Hydrol.* **526**, 253–264 (2015).
22. Lin, W., Wen, C., Wen, Z. & Gang, H. Drought in Southwest China: a review. *Atmos. Ocean. Sci. Lett.* **8**, 146 (2015).
23. Mokhtar, A. et al. Ecosystem water use efficiency response to drought over Southwest China. *Ecohydrology.* **15**, https://doi.org/10.1002/eco.2317. (2021).
24. Mokhtar, A. et al. Estimation of SPEI meteorological drought using machine learning algorithms. *IEEE Access* **9**, 65503–65523 (2021).
25. Li, Y., Xu, H. & Liu, D. Features of the extremely severe drought in the east of southwest china and anomalies of atmospheric circulation in summer 2006. *Acta Meteorol. Sin.* **25**, 176–187 (2011).
26. Barriopedro, D., Gouveia, C. M., Trigo, R. M. & Wang, L. The 2009/10 drought in China: possible causes and impacts on vegetation. *J. Hydrometeorol.* **13**, 1251–1267 (2012).
27. Yang, J., Gong, D., Wang, W., Hu, M. & Mao, R. Extreme drought event of 2009/2010 over southwestern China. *Meteorol. Atmos. Phys.* **115**, 173–184 (2012).
28. Jinghua, Z., Luguang, J., Zhiming, F. & Peng, L. Detecting effects of the recent drought on vegetation in Southwestern China. *J. Resour. Ecol.* **3**, 43–49 (2012).
29. Zhang, L. et al. The 2010 spring drought reduced primary productivity in southwestern China. *Environ. Res. Lett.* **7**, 045706 (2012).
30. Mokhtar, A. et al. Estimation of the rice water footprint based on machine learning algorithms. *Comput. Electron. Agric.* **191**, 106501 (2021).
31. West, H., Quinn, N. & Horswell, M. Remote sensing for drought monitoring & impact assessment: Progress, past challenges and future opportunities. *Remote Sens. Environ*. **232**, 111291 (2019).
32. Wilhite, D. A. & Glantz, M. H. Understanding: The drought phenomenon: The role of definitions. *Water Int* **10**, 111–120 (1985).
33. Van Loon, A. F. Hydrological drought explained. *Wiley Interdiscip. Rev. Water* **2**, 359–392 (2015).
34. Wong, G., van Lanen, H. A. J. & Torfs, P. J. J. F. Probabilistic analysis of hydrological drought characteristics using meteorological drought. *Hydrol. Sci. J.* **58**, 253–270 (2013).
35. Xu, Z., Wu, Z., Shao, Q., He, H. & Guo, X. From meteorological to agricultural drought: Propagation time and probabilistic linkages. *J. Hydrol. Reg. Stud.* **46**, 101329 (2023).
36. Cao, S. et al. Effects and contributions of meteorological drought on agricultural drought under different climatic zones and vegetation types in Northwest China. *Sci. Total Environ.* **821**, 153270 (2022).
37. Leng, G., Tang, Q. & Rayburg, S. Climate change impacts on meteorological, agricultural and hydrological droughts in China. *Glob. Planet. Change* **126**, 135299 (2015).

38. Dai, A., Zhao, T. & Chen, J. Climate change and drought: a precipitation and evaporation perspective. *Curr. Clim. Change Rep.* **4**, 301–312 (2018).

39. Herrera, D. A. et al. Exacerbation of the 2013–2016 Pan-Caribbean Drought by Anthropogenic Warming. *Geophys. Res. Lett.* **45**, 10619–10626 (2018).

40. Zhang, X. et al. Drought propagation under global warming: Characteristics, approaches, processes, and controlling factors. *Sci. Total Environ.* **838**, 156021 (2022).

41. AghaKouchak, A. et al. Anthropogenic drought: definition, challenges, and opportunities. *Rev. Geophys*. **59**, https://doi.org/10.1029/2019RG000683 (2021).

42. Vicente-Serrano, S. M. et al. High temporal variability not trend dominates Mediterranean precipitation. *Nature* **639**, 658–666 (2025).

43. Chiang, F., Mazdiyasni, O. & AghaKouchak, A. Evidence of anthropogenic impacts on global drought frequency, duration, and intensity. *Nat. Commun.* **12**, 2754 (2021).

44. Zhao, R., Sun, H., Xing, L., Li, R. & Li, M. Effects of anthropogenic climate change on the drought characteristics in China: from frequency, duration, intensity, and affected area. *J. Hydrol.* **617**, 129008 (2023).

45. Dai, R., Huang, J., Chen, Z., Zhou, J. & Havea, P. H. Impacts of anthropogenic climate change on meteorological drought in China. *Front. Earth Sci*. **12**, 1369523 (2024).

46. Dai, A. Increasing drought under global warming in observations and models. *Nat. Clim. Chang.* **3**, 52–58 (2013).

47. Gong, Y., Wei, Y. & Gu, J. Urbanisation of the Chinese rural population: a literature review of China's new-type urbanisation. *China An Int. J.* **20**, 181–204 (2022).

48. Ruibo, H. & Linna, W. Challenges and opportunities facing China's urban development in the new era. *China Perspect*. **2013**, 26317745241270568, (2013).

49. Wu, J., Xiang, W.-N. & Zhao, J. Urban ecology in China: historical developments and future directions. *Landsc. Urban Plan.* **125**, 209–221 (2014).

50. Huang, S. et al. Urbanization amplified asymmetrical changes of rainfall and exacerbated drought: analysis over five urban agglomerations in the Yangtze River Basin, China. *Earth's Futur*. **11**, e2022EF003117 (2023).

51. Elmqvist, T. et al. Urbanization in and for the Anthropocene. *npj Urban Sustain.* **1**, 6 (2021). at.

52. Ndehedehe, C. E. et al. Global assessment of drought characteristics in the Anthropocene. *Resour. Environ. Sustain* **12**, 100105 (2023).

53. Mu, Y. et al. Analysis of the ongoing effects of disasters in urbanization process and climate change: China's floods and droughts. *Sustain*. **16**, 14 (2024).

54. Huang, S. et al. Urbanization-induced spatial and temporal patterns of local drought revealed by high-resolution fused remotely sensed datasets. *Remote Sens. Environ.* **313**, 114378 (2024).

55. Sun, J. et al. Historical trends and characteristics of meteorological drought based on standardized precipitation index and standardized precipitation evapotranspiration index over the past 70 years in China (1951–2020). *Sustainability* **15**, 10875 (2023).

56. Luo, S. et al. Anthropogenic climate change and urbanization exacerbate risk of hybrid heat extremes in China. *J. Geophys. Res. Atmos.* **129**, e2024JD041568 (2024).

57. Trenberth, K. E. Changes in precipitation with climate change. *Clim. Res.* **47**, 123–138 (2011).

58. Wu, S. et al. Urbanization-driven increases in summertime compound heat extremes across China. *Sci. Total Environ.* **799**, 149166 (2021).

59. Li, Y., Schubert, S., Kropp, J. P. & Rybski, D. On the influence of density and morphology on the Urban Heat Island intensity. *Nat. Commun.* **11**, 2647 (2020).

60. Chen, Z. & Zhang, Y. Quantitative Identification of Temporal-Spatial Variations of Urban Heat Island (UHI) Effects in Changchun, China. *IEEE J. Sel. Top. Appl. Earth Obs. Remote Sens.* **15**, 3052–3060 (2022).

61. Ouyang, Z. et al. Albedo changes caused by future urbanization contribute to global warming. *Nat. Commun.* **13**, 3800 (2022).

62. Zhang, Z. et al. A mechanistic assessment of urban heat island intensities and drivers across climates. *Urban Clim* **44**, 101215 (2022).

63. Han, L. et al. Impacts of long-term urbanization on summer rainfall climatology in Yangtze river delta agglomeration of China. *Geophys. Res. Lett.* **49**, e2021GL097546 (2022).

64. Lalonde, M., Oudin, L. & Bastin, S. Urban effects on precipitation: do the diversity of research strategies and urban characteristics preclude general conclusions?. *Urban Clim* **51**, 101605 (2023).

65. Shastri, H., Paul, S., Ghosh, S. & Karmakar, S. Impacts of urbanization on Indian summer monsoon rainfall extremes. *J. Geophys. Res.* **120**, 496–516 (2015).

66. Ma, S., Zhou, T., Dai, A. & Han, Z. Observed changes in the distributions of daily precipitation frequency and amount over China from 1960 to 2013. *J. Clim.* **28**, 6960–6978 (2015).

67. Akinyoola, J. A., Oluleye, A. & Gbode, I. E. A review of atmospheric aerosol impacts on regional extreme weather and climate events. *Aerosol Sci. Eng.* **8**, 249–274 (2024).

68. Wang, Z. et al. Roles of atmospheric aerosols in extreme meteorological events: a systematic review. *Curr. Pollution Rep.* **8**, 177–188 (2022). at.

69. Wang, J. et al. Modulations of dust aerosols on precipitation: evidence from a typical heavy sandstorm event. *Atmos. Res.* **304**, 107411 (2024).

70. Shao, T. et al. Role of anthropogenic aerosols in affecting different-grade precipitation over eastern China: a case study. *Sci. Total Environ.* **807**, 150886 (2022).

71. Huang, S. et al. Widespread global exacerbation of extreme drought induced by urbanization. *Nat. Cities* **1**, 597–609 (2024).

72. Alsafadi, K., Mohammed, S. A., Ayugi, B., Sharaf, M. & Harsányi, E. Spatial–temporal evolution of drought characteristics over Hungary between 1961 and 2010. *Pure Appl. Geophys.* **177**, 3961–3978 (2020).

73. Wang, S. et al. Drought evolution characteristics of the Qinghai-Tibet Plateau over the last 100 years based on SPEI. *Nat. Hazards Earth Syst. Sci. Discuss*. **2021**, 1–20 (2021).

74. Yu, M., Li, Q., Hayes, M. J., Svoboda, M. D. & Heim, R. R. Are droughts becoming more frequent or severe in China based on the standardized precipitation evapotranspiration index: 1951-2010?. *Int. J. Climatol.* **34**, 545–558 (2014).

75. Liang, C. et al. Assessing urban flood and drought risks under climate change, China. *Hydrol. Process.* **33**, 1349–1361 (2019).

76. Wen, Q. & Chen, H. Changes in drought characteristics over China during 1961–2019. *Front. Earth Sci.* **11**, 143 (2023).

77. Chen, H. & Sun, J. Changes in drought characteristics over china using the standardized precipitation evapotranspiration index. *J. Clim.* **28**, 5430–5447 (2015).

78. Jiang, M., Li, Z., Wan, B. & Cribb, M. Impact of aerosols on precipitation from deep convective clouds in eastern China. *J. Geophys. Res.* **121**, 9607–9620 (2016).

79. Fan, J., Zhang, Y., Li, Z., Hu, J. & Rosenfeld, D. Urbanization-induced land and aerosol impacts on sea-breeze circulation and convective precipitation. *Atmos. Chem. Phys.* **20**, 14163–14182 (2020).

80. Tao, W. K., Chen, J. P., Li, Z., Wang, C. & Zhang, C. Impact of aerosols on convective clouds and precipitation. *Rev. Geophys.* **50**, RG2001 (2012).

81. Zhang, L., Chen, X. & Lai, R. Urban signatures of sub-daily extreme precipitation events over a metropolitan region. *Atmos. Res.* **246**, 5382–5389 (2020).

82. Marelle, L. et al. Urbanization in megacities increases the frequency of extreme precipitation events far more than their intensity. *Environ. Res. Lett.* **15**, 124072 (2020).

83. Liu, H., Zou, L., Xia, J., Chen, T. & Wang, F. Impact assessment of climate change and urbanization on the nonstationarity of extreme precipitation: a case study in an urban agglomeration in the middle reaches of the Yangtze river. *Sustain. Cities Soc.* **85**, 104061 (2022).

84. Luo, M. & Lau, N. C. Urban expansion and drying climate in an urban agglomeration of East China. *Geophys. Res. Lett.* **46**, 6868–6877 (2019).

85. Hao, L. et al. Urbanization alters atmospheric dryness through land evapotranspiration. *npj Clim. Atmos. Sci.* **6**, 149 (2023).

86. Huang, S. et al. Urbanization-induced drought modification: example over the Yangtze River Basin, China. *Urban Clim* **44**, 101231 (2022).

87. Yuan, J. et al. Influence of global warming and urbanization on regional climate of megacity: a case study of Chengdu, China. *Urban Clim* **44**, 101227 (2022).

88. Shen, P., Zhao, S., Ma, Y. & Liu, S. Urbanization-induced Earth's surface energy alteration and warming: a global spatiotemporal analysis. *Remote Sens. Environ.* **284**, 113361 (2023).

89. Shen, P., Zhao, S. & Ma, Y. Perturbation of Urbanization to Earth's Surface Energy Balance. *J. Geophys. Res. Atmos*. **126**, e2020JD033521 (2021).

90. Zhao, L., Lee, X., Smith, R. B. & Oleson, K. Strong contributions of local background climate to urban heat islands. *Nature* **511**, 216–219 (2014).

91. Westra, S. et al. Future changes to the intensity and frequency of short-duration extreme rainfall. *Rev. Geophys.* **52**, 522–555 (2014). at.

92. Yang, L., Tian, F., Smith, J. A. & Hu, H. Urban signatures in the spatial clustering of summer heavy rainfall events over the Beijing metropolitan region. *J. Geophys. Res. Atmos.* **119**, 1203–1217 (2014).

93. Zhang, Y., Miao, S., Dai, Y. & Bornstein, R. Numerical simulation of urban land surface effects on summer convective rainfall under different UHI intensity in Beijing. *J. Geophys. Res. Atmos.* **122**, 7851–7868 (2017).

94. Rosenfeld, D. et al. Global observations of aerosol-cloud-precipitation-climate interactions. *Rev. Geophys.* **52**, 750–808 (2014). at.

95. Teller, A. & Levin, Z. The effects of aerosols on precipitation and dimensions of subtropical clouds: A sensitivity study using a numerical cloud model. *Atmos. Chem. Phys.* **6**, 67–80 (2006).

96. Jiang, Y., Liu, X., Yang, X. Q. & Wang, M. A numerical study of the effect of different aerosol types on East Asian summer clouds and precipitation. *Atmos. Environ.* **70**, 51–63 (2013).

97. Salah, Z., Steiner, A., Zakey, A. S., Shalaby, A. & Wahab, M. M. A. An exploration of the aerosol indirect effects in East Asia using a regional climate model. *Atmosfera* **33**, 87–103 (2020).

98. Fan, J. et al. Substantial contribution of anthropogenic air pollution to catastrophic floods in Southwest China. *Geophys. Res. Lett.* **42**, 6066–6075 (2015).

99. Zhang, Y., Yu, F., Luo, G., Chen, J. P. & Chou, C. C. K. Impact of mineral dust on summertime precipitation over the Taiwan Region. *J. Geophys. Res. Atmos*. **125**, e2020JD033120 (2020).

100. Fan, J. et al. Substantial convection and precipitation enhancements by ultrafine aerosol particles. *Science* **359**, 411–418 (2018).

101. Adhikari, P. & Mejia, J. F. Aerosol-precipitation elevation dependence over the central Himalayas using cloud-resolving WRF-Chem numerical modeling. *Atmos. Chem. Phys.* **23**, 1019–1042 (2023).

102. Naeger, A. R. Impact of dust aerosols on precipitation associated with atmospheric rivers using WRF-Chem simulations. *Results Phys.* **10**, 217–221 (2018).

103. Sun, Y., Zhang, X., Ren, G., Zwiers, F. W. & Hu, T. Contribution of urbanization to warming in China. *Nat. Clim. Chang.* **6**, 706–709 (2016).

104. Lobo, J. et al. Integration of urban science and urban climate adaptation research: opportunities to advance climate action. *npj Urban Sustain.* **3**, 32 (2023).

105. Zhou, D., Zhao, S., Liu, S., Zhang, L. & Zhu, C. Surface urban heat island in China's 32 major cities: spatial patterns and drivers. *Remote Sens. Environ.* **152**, 101–106 (2014).

106. Abulimiti, A. et al. Urbanization effect on local summer climate in arid region city of Urumqi: a numerical case study. *Remote Sensing* **17**, 476 (2025). at.

107. Li, J. et al. East Asian climate under global warming: understanding and projection. *Clim. Dyn.* **51**, 3969–3972 (2018). at.

108. Piao, S. et al. The impacts of climate change on water resources and agriculture in China. *Nature* **467**, 43–51 (2010). at.

109. Wang, B. & Ho, L. Rainy season of the Asian-Pacific summer monsoon. *J. Clim.* **15**, 386–398 (2002).

110. Qian, W., Kang, H. S. & Lee, D. K. Distribution of seasonal rainfall in the East Asian monsoon region. *Theor. Appl. Climatol.* **73**, 151–168 (2002).

111. Schamm, K. et al. Global gridded precipitation over land: a description of the new GPCC First Guess Daily product. *Earth Syst. Sci. Data* **6**, 49–60 (2014).

112. Harris, I., Osborn, T. J., Jones, P. & Lister, D. Version 4 of the CRU TS monthly high-resolution gridded multivariate climate dataset. *Sci. Data* **7**, 109 (2020).

113. Vicente-Serrano, S. M., Beguería, S. & López-Moreno, J. I. A multiscalar drought index sensitive to global warming: The standardized precipitation evapotranspiration index. *J. Clim.* **23**, 1696–1718 (2010).

114. Ma, B., Zhang, B., Jia, L. & Huang, H. Conditional distribution selection for SPEI-daily and its revealed meteorological drought characteristics in China from 1961 to 2017. *Atmos. Res.* **246**, 105108 (2020).

115. Mann, H. B. & Mann Nonparametric test against trend. *Econometrica* **13**, 245–259 (1945).

116. Kendall, M. G. *Rank Correlation Methods (4th Edn.) Charles Griffin*. *San Francisco, CA* (1975).

117. Hamed, K. H. & Ramachandra Rao, A. A modified Mann-Kendall trend test for autocorrelated data. *J. Hydrol.* **204**, 182–196 (1998).

118. Theil, H. A Rank-Invariant Method of linear and polynomial regression analysis. 345–381, https://doi.org/10.1007/978-94-011-2546-8_20. (1992).

119. Sen, P. K. Estimates of the regression coefficient based on Kendall's Tau. *J. Am. Stat. Assoc.* **63**, 1379–1389 (1968).

120. Hannaford, J., Buys, G., Stahl, K. & Tallaksen, L. M. The influence of decadal-scale variability on trends in long European streamflow records. *Hydrol. Earth Syst. Sci.* **17**, 2717–2733 (2013).

121. Serrano, A., García, J. A., Mateos, V. L., Cancillo, M. L. & Garrido, J. Monthly modes of variation of precipitation over the Iberian Peninsula. *J. Clim.* **12**, 2894–2919 (1999).

122. Yevjevich, V. M. An objective approach to definitions and investigations of continental hydrologic droughts. VUJICA YEVJEVICH: Fort Collins, Colorado State University, 1967, 19 p. (Hydrology paper no. 23). *J. Hydrol.* **7**, 353 (1967).

123. Liu, X. et al. Regionalization and spatiotemporal variation of drought in China based on standardized precipitation evapotranspiration index (1961-2013). *Adv. Meteorol.* **2015**, 1–18 (2015).

124. Lee, S. H., Yoo, S. H., Choi, J. Y. & Bae, S. Assessment of the impact of climate change on drought characteristics in the Hwanghae Plain, North Korea using time series SPI and SPEI: 1981–2100. *Water* **9**, 579 (2017).

125. McKee, T. B., Nolan, J. & Kleist, J. The relationship of drought frequency and duration to time scales. In *Proc. 8th Conference on Applied Climatology* (Dallas, TX) 233–236 (1993).

126. Zhang, L. et al. Drought events and their effects on vegetation productivity in China. *Ecosphere* **7**, e01591 (2016).
127. Salvadori, G., Durante, F., De Michele, C., Bernardi, M. & Petrella, L. A multivariate copula-based framework for dealing with hazard scenarios and failure probabilities. *Water Resour. Res.* **52**, 3701–3721 (2016).
128. Yin, J. et al. A meta-heuristic approach for multivariate design flood quantile estimation incorporating historical information. *Hydrol. Res.* **50**, 526–544 (2019).
129. Akaike, H. A new look at the statistical model identification. *IEEE Trans. Automat. Contr.* **19**, 716–723 (1974).
130. Shiau, J. T. Return period of bivariate distributed extreme hydrological events. *Stoch. Environ. Res. Risk Assess.* **17**, 42–57 (2003).
131. Sadegh, M. et al. Multihazard scenarios for analysis of compound extreme events. *Geophys. Res. Lett.* **45**, 5470–5480 (2018).
132. Ullah, I. et al. Projected changes in increased drought risks over South Asia under a warmer climate. *Earth's Futur.* **10**, e2022EF002830 (2022).
133. Ullah, I. et al. Anthropogenic and atmospheric variability intensifies flash drought episodes in South Asia. *Commun. Earth Environ.* **5**, 267 (2024).
134. Pandey, V., Pandey, P. K. & Lalrammawii, H. P. Characterization and return period analysis of meteorological drought under the humid subtropical climate of Manipur, northeast India. *Nat. Hazards Res.* **3**, 546–555 (2023).
135. Gu, L. et al. Projected increases in magnitude and socioeconomic exposure of global droughts in 1.5 and 2 °C warmer climates. *Hydrol. Earth Syst. Sci.* **24**, 451–472 (2020).
136. Gräler, B. et al. Multivariate return periods in hydrology: a critical and practical review focusing on synthetic design hydrograph estimation. *Hydrol. Earth Syst. Sci.* **17**, 1281–1296 (2013).
137. Ren, H., Huang, X., Yang, J. & Zhou, G. Improving 30-meter global impervious surface area (GISA) mapping: new method and dataset. *ISPRS J. Photogramm. Remote Sens.* **220**, 354–376 (2025).
138. Ren, G. & Zhou, Y. Urbanization effect on trends of extreme temperature indices of national stations over mainland China, 1961-2008. *J. Clim.* **27**, 2340–2360 (2014).
139. Liao, W. et al. Stronger contributions of urbanization to heat wave trends in wet climates. *Geophys. Res. Lett.* **45**, 11–310 (2018).
140. Yu, X. et al. Asymmetrical shift toward less light and more heavy precipitation in an urban agglomeration of East China: Intensification by urbanization. *Geophys. Res. Lett.* **49**, e2021GL097046 (2022).
141. Yang, Y. et al. Anthropogenic emissions and urbanization increase risk of compound hot extremes in cities. *Nat. Clim. Chang.* **11**, 15153–15163 (2021).

Acknowledgements

Author contributions

Author contributions: K.A. conceptualized the study, developed the methodology, and handled visualization. K.A. and J.S. contributed to codes development. K.A. and I.U. performed the formal analysis. K.A. was responsible for the investigation. J.S. and S.B. managed the data curation. K.A., J.S., and B.R.L. prepared the original draft of the manuscript. W.C., S.Y., F.E., F.W., and A.K.S. contributed to the writing—review and editing of the manuscript. W.C. provided supervision and secured funding acquisition. All authors contributed to reviewing and approving the final version of the manuscript.

Competing interests

The authors declare no competing interests.

Additional information

Supplementary information The online version contains supplementary material available at https://doi.org/10.1038/s42949-025-00267-z.

Correspondence and requests for materials should be addressed to Karam Alsafadi or Wenzhi Cao.

Reprints and permissions information is available at http://www.nature.com/reprints

Publisher's note Springer Nature remains neutral with regard to jurisdictional claims in published maps and institutional affiliations.